https://doi.org/10.5194/egusphere-2026-4592
Preprint. Discussion started: 20 August 2026

Compound Flooding in Surabaya: A Multi-driver Sensitivity and Interaction Analysis

Agustia Larasari[1], Johan Reyns[2,3,4], Khin Nawarat[2,5], Ali Dastgheib[2,6,7]

1 Department of Civil and Resource Engineering, Dalhousie University, Halifax, Canada
2 Coastal and Urban Risk & Resilience Department, IHE Delft, Delft, the Netherlands
3 Deltares, Delft, the Netherlands
4 Faculty of Civil Engineering and Geosciences, Delft University of Technology, Delft, the Netherlands
5 University of Twente, Enschede, The Netherlands
6 International Marine and Dredging Consultants, Antwerp, Belgium
7 Department of Civil Engineering, Institut Teknologi Sepuluh Nopember, Surabaya, Indonesia

Correspondence to: Agustia Larasari (a.larasari@dal.ca)

Abstract. Coastal compound flooding, caused by interactions between various flood drivers, presents serious threats to urban coastal regions. In this study, a process-based modelling framework was applied by integrating statistical analysis of historical data with reduced-physics numerical simulations to assess compound flood hazards. A very low correlation between extreme sea level and heavy rainfall events in the study area was demonstrated, which confirmed the initial assumption of flood driver independence. Single-driver and compound-driver scenarios corresponding to a 100-year return period were simulated for present-day and future conditions, accounting for relative sea-level rise and intensified extreme rainfall under SSP2-4.5 and SSP5-8.5 by 2100. Results indicate that non-linear interactions between drivers lead to a considerable amplification of flood hazards. The primary impact mechanism is increased inundation depth within existing floodplains due to backwater effects, which affects 8.6% to 20.9% (10.7 to 36.6 km^2) of the total inundated area. A secondary effect is the expansion of the flood extent into previously unaffected areas by 0.82% to 1.1% (1 to 1.7 km^2) of the total inundated area. Climate change is projected to exacerbate these hazards substantially. Under the high-emission SSP5-8.5 scenario, a coastal compound event with a current 100-year return period is projected to occur as frequently as every 2-3 years by 2100. This dramatic increase in frequency, along with a substantial rise in flood intensity, is primarily driven by sea-level rise.

1 Introduction

Compound flooding occurs when two or more flood drivers act simultaneously, resulting in a greater impact due to their interactions. While compound floods can result from a single meteorological event, such as a tropical cyclone, they can also result from multiple separate events occurring either in close succession or simultaneously (Santiago-Collazo et al., 2019). The study of coastal compound flooding has received growing attention because of the increasing frequency and severity of oceanographic, hydrologic, and meteorological extremes driven by climate change (Jalili Pirani and Najafi, 2020; Patricola and Wehner, 2018; Zscheischler et al., 2018a). Long-term, slow-onset processes like rising sea levels and land subsidence also

https://doi.org/10.5194/egusphere-2026-4592
Preprint. Discussion started: 20 August 2026

contribute to increased coastal flooding (Nicholls et al., 2021). Meanwhile, global warming is expected to drive more extreme rainfall events, as higher evaporation increases atmospheric moisture, changing precipitation patterns and intensifying downpours (IPCC, 2023; Trenberth et al., 2003). Due to its amplified impacts compared with single-source flooding, compound flooding is especially concerning in densely populated urban coastal areas, where concentrated infrastructure and communities are at high risk of flooding (Ganguli and Merz, 2019; Wahl et al., 2015).

The city of Surabaya in Indonesia has known compound flooding problems for centuries (Tantri, 2018). The larger part of the city lies at the end of the Brantas River delta, in a predominantly flat to gently sloping area (0–8% slope) with elevations ranging from 0 to 6 meters above sea level, making it particularly susceptible to flooding during the rainy season and periodical spring tide (Safitri et al., 2024; Indonesian Agency for Meteorology, Climatology, and Geophysics, 2025). At present, Surabaya, like other major coastal cities, faces growing vulnerability to coastal flooding due to a combination of natural and anthropogenic factors, such as high population density and extensive built-up areas (Pamungkas and Purwitaningsih, 2021; Prawira and Pamungkas, 2014; Triana and Hidayah, 2020). In addition, a positive historical trend in the frequency and intensity of extreme rainfall in Surabaya during 1979-2010 was documented by Supari (2012). Intense rainfall in the upstream catchments of the Brantas river and its tributaries often strains the capacity of urban drainage systems due to reduced infiltration rates and the increase in surface runoff (Savitri et al., 2022).

In the long run, the vulnerability to coastal flooding in Surabaya is further exacerbated by sea level rise (SLR) (Damayanti, 2016; Sulma et al., 2013) and land subsidence in the northern and eastern parts of the city (Ardha et al., 2022; Riastama et al., 2023).

Despite this susceptibility to single and combined flood drivers, the mechanism behind compound flood events in Surabaya remains underinvestigated, particularly in the context of the present and future changing climate.

In this study, we investigated various scenarios for the drivers of compound floods, including the effects of climate change by 2100 for the specific case of Surabaya. First, we explore the relationship between extreme sea level and rainfall intensity to understand how it affects the joint probability of coastal compound flooding. Based on the aforementioned statistical relationship between flood drivers, a set of single-driver and compound-driver flooding scenarios was constructed and assigned an equiprobable return period. The interactions between flood drivers were analyzed based on metrics like flooded area and depth simulated by the reduced-physics numerical model SFINCS (Leijnse et al., 2021). We also assess the influence of future relative sea level rise (RSLR) and increasing rainfall intensity under the SSP2-4.5 and SSP5-8.5 scenarios on the frequency and severity of coastal compound flooding events by the end of 21st century.

2 Study area

Surabaya is the capital of East Java Province in Indonesia. The city is strategically positioned on the north-eastern corner of Java Island at -7.24°S, 112.73°E. The city covers an area of about 350 km^2. It occupies the low-lying Brantas River Delta, where the Surabaya River and Mas River converge before flowing into the Madura Strait. Rather than directly facing the Java

https://doi.org/10.5194/egusphere-2026-4592
Preprint. Discussion started: 20 August 2026

Sea, Surabaya primarily overlooks the Madura Strait on its north-eastern side. At approximately 3 km across the Strait, Madura Island shelters the city from the open ocean (Figure 1). The area experiences a tropical climate, with a mean annual rainfall of 1518 mm. The rainy season extends from October to May, peaking in January (mean monthly precipitation 288 ± 100 mm) and February (281 ± 85 mm) (Indonesian Agency for Meteorology, Climatology, and Geophysics, 2025). The coastal region is characterized by a mixed, predominantly semidiurnal tidal regime (Fitriana et al., 2022). Periodical spring tides exceeding 1.5 meters above mean sea level (MSL), heavily threaten low-lying areas in the northern and eastern parts of Surabaya (Agency for Meteorology, Climatology, and Geophysics, 2024; Anjasmara et al., 2020). This inundation risk is severely compounded by localized land subsidence ranging from 0.2–83.3 mm/year, which rapidly drives down land elevation and accelerates RSLR, allowing tidal floods to extend much further inland (Riastama et al., 2023). To mitigate pluvial flooding and facilitate river drainage to the sea, the city is equipped with urban drainage and flood control systems, as extensively discussed in Nayadiah (2011) and Susetyo (2008).

Figure 1: The study area of Surabaya City, East Java, including the locations of the meteorological and oceanographic data sources. Surabaya river, Wonokromo river, and Mas river flows are highlighted with a light blue line crossing the city east and north direction toward Madura Strait. Hydrology and oceanographic data sources are situated within the Tanjung Perak Port area of Surabaya, as shown in the upper right inset. Microsoft product screen shot(s) reprinted with permission from Microsoft Corporation.

3 Methods

To investigate the combined impact of rainfall intensity and coastal water levels on compound flooding, we employ a process-based hydrodynamic modelling framework to complement the statistical analysis of extreme flood drivers. This approach enables the explicit examination of nonlinear interactions within the river system and drainage network.

https://doi.org/10.5194/egusphere-2026-4592
Preprint. Discussion started: 20 August 2026

The assessment follows a scenario-based strategy, in which the SFINCS model is forced with a selection of synthetic design events derived from extreme-value analysis. As detailed in the workflow (Figure 2), the methodology is structured into three distinct phases: 1) Statistical analysis of input data, which defines the boundary conditions based on extreme value analysis (EVA) and statistical correlation between flood drivers; 2) Numerical modeling, covering the model setup and simulation of single and compound driver scenarios; and 3) Flood hazard assessment, where amplification effects were quantified through spatial analysis. Rainfall and sea level datasets were used to represent flood drivers within the study area. Recorded daily rainfall was collected from Tanjung Perak Meteorological Station and 10-minute coastal water level was obtained from Muis et al. (2022) (Table 1).

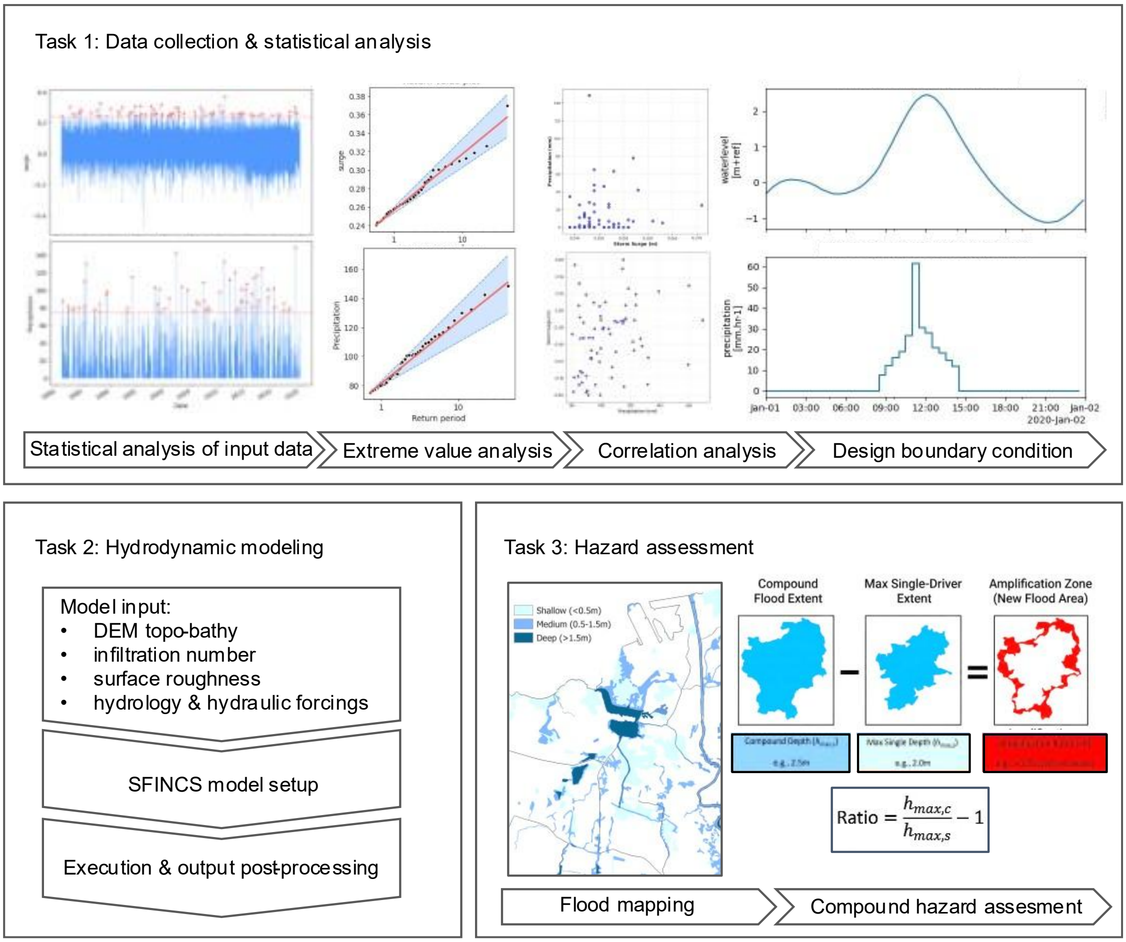

Figure 2: The study workflow is organized into three main tasks. The first involves statistical analysis of long-term rainfall and coastal water level time series data, identifying extreme events and assessing the statistical dependence between rainfall and sea level extremes. The resulting return periods from EVA were used to define boundary conditions in the 24-hour simulations. The second task focuses on preparing the domain setup and defining the physical properties of the hydrodynamic model. Each simulation generates a map of maximum flood extent and depth. The final task includes hazard assessment through spatial analysis for every scenario. Flood extent and depth were quantified to evaluate the impacts of individual and compound flooding drivers.

https://doi.org/10.5194/egusphere-2026-4592
Preprint. Discussion started: 20 August 2026

Table 1. Data source for the main flood drivers

Variable	Station name - ID	Latitude	Longitude	Data length	Temporal resolution
Daily rainfall	Tanjung Perak - WMO 962937	-7.2053	112.7353	1981-2024	Daily
Coastal water level	GTSM - Station 39053	-7.192	112.72	1981-2024	10-minute

3.1 Input data

We used long-term continuous observational and reanalysis data for statistical analysis of historical compound flood events in the study area. Daily rainfall data from 1981 to 2024 was obtained from the Maritime Meteorological Station at Tanjung Perak, Surabaya, which is managed by the Indonesian Agency for Meteorology, Climatology, and Geophysics (2025). This station was chosen because it has the longest quality-controlled records (44 years). Continuous records of daily rainfall were recorded in milimeters and zero represented days with no rainfall. No stations within the study area have a sub-daily precipitation record. Sea-level data, covering from 1981 to 2024, was derived from the Global Tide and Surge Model (GTSM) forced by the sea level related atmospheric variables from ERA5 reanalysis dataset (Muis et al., 2022). This dataset includes coastal water levels modelled at 10-minute intervals, capturing key components such as astronomical tides, storm surges, and MSL. Storm surge component used in the subsequent analysis was derived from the GTSM dataset. In this study, we focus on the storm surge component for further statistical analysis because it is the stochastic part that contributes to extreme total water levels.

3.2 Extreme value analysis

Return values and corresponding return periods of independent extreme rainfall and storm surge events were estimated through EVA. The Peak-Over-Threshold (POT) method was chosen to select the extreme values across the entire dataset. The selected extremes were then fitted to the Generalized Pareto Distribution to estimate storm surge heights and rainfall amounts for selected return periods, i.e., 1, 5, 10, 20, and 100 years. For rainfall, a threshold of 75 mm (equal to the 99.5% quantile) was used to define events as extreme, while for the storm surge variable, a threshold of 0.24 meters (equal to the 99.95% quantile) was used as input to the analysis. 168-hour (5-day) windows was used to separate those events to ensure they are independent and identically distributed (i.i.d). An exponential form of the Generalized Pareto distribution (shape parameter ξ fixed at zero) was fitted to the exceedances of each variable by maximum-likelihood estimation and validated using quantile-quantile and probability-probability plots.

3.3 Correlation analysis

Correlation analysis was conducted to determine the statistical dependence between extreme rainfall and extreme sea level events. To isolate the meteorological component, astronomical tides were removed from the sea level records, leaving the non-tidal residuals (surge) which superimposed by historical SLR. Pairs of high-quantile rainfall events with the highest surge (both exceeding 95th percentile and treated as i.i.d events) occurring within ±1 day were selected to account for the typical lag in

https://doi.org/10.5194/egusphere-2026-4592
Preprint. Discussion started: 20 August 2026

compound coastal-pluvial events. Dependence was assessed using Kendall's rank correlation coefficient (τ). This metric was chosen because it is non-parametric and robust to the non-normal distributions typical of extreme hydrological data. The interpretation of correlation coefficient values follows standard guidelines (Higgins, 2004): below +0.1 indicates a very weak correlation, +0.1 to +0.3 is considered a weak correlation, +0.3 to +0.5 suggests a moderate correlation, +0.5 to +0.7 indicates a strong correlation, and above +0.7 up to +1.0 signifies a very strong correlation. A p-value threshold of 0.05 was used to identify statistically significant correlation between variables.

3.4 Boundary condition representation

Typical storm-surge and rainfall time series were generated for the selected return periods to simulate conservative flood scenarios and their potential impacts. A parameterized temporal pattern was applied to storm surge return values to represent storm surge conditions based on the reanalysis dataset (Pineau-Guillou et al., 2023). The typical surge shape was derived by averaging the time series of the top 82 highest POT surge events in the reanalysis record, which exceeded a threshold of 0.24 meters (equal to 99.95% quantile). Subsequently, the non-tidal surge residuals were represented separately from the astronomical tide. An amplification method was applied to magnify the typical residual shape to match extreme event return values (Xu et al., 2024). To reconstruct the Total Water Level (TWL) for boundary condition, this amplified surge residual was superposed onto the Highest Astronomical Tide (HAT). For the design extreme rainfall events, Intensity-Duration-Frequency curves were derived using the Van Breen method to calculate the six-hour total rainfall for selected return periods (Brotowiryatmo, 2016; Khansa et al., 2020). A typical extreme-rainfall event was derived based on sub-daily rainfall patterns from satellite data and then scaled using the same method as the one used for the storm surge residuals. Although statistical independence between drivers was demonstrated (4.1 Statistical Analysis), the peak rainfall and storm surge were perfectly aligned to create a conservative worst-case design event. To isolate these coastal-pluvial dynamics, our modeling approach purposefully omitted a dynamic, upstream river flood wave; instead, the main river system is held at a constant, conservative bankfull discharge to simulate pre-existing wet-season constraints. This boundary condition ensures that any additional simulated flooding is driven entirely by extremes overlap between coastal and meteorological forcings (Figure 3), rather than regional fluvial propagation. The spatial-temporal progression and hydrodynamic implications of the forcings response lag are verified and evaluated further within the driver dominance framework in the discussion section (5.3 Driver dominance).

To include expected future climate change impacts on flood drivers, a projected value of RSLR and rainfall intensification was applied under the SSP2-4.5 and SSP5-8.5 scenarios for the year 2100. The local RSLR was obtained from Vousdoukas et al. (2018) and was set at a median value of +0.57 m for SSP2 4.5 and +0.92 m for SSP5-8.5, relative to baseline sea levels. Rainfall intensification was derived from projections of extreme wet-season rainfall indices across most of Indonesia for the far-future periods (Kurniadi et al., 2024) and estimated to increase by +17.44% and +23.61%.

https://doi.org/10.5194/egusphere-2026-4592
Preprint. Discussion started: 20 August 2026

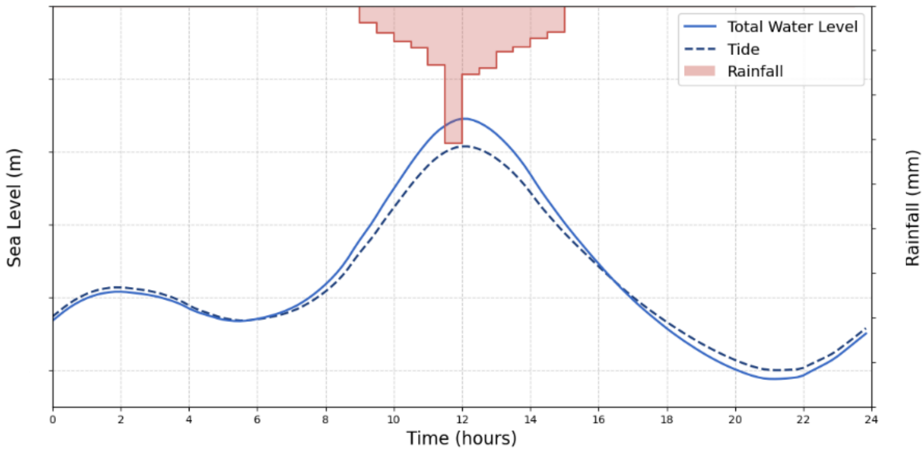

Figure 3: Schematic illustration of the boundary conditions construction. Independent rainfall and storm surge time series were scaled to their respective design return periods (e.g., 10-year storm and 10-year surge, denoted as the R10W10 scenario, for a 100-year compound scenario) and aligned in time. The peak coincidence represents a conservative assumption for determining the 100-year joint flood hazard.

3.5 Hydrodynamic modelling using SFINCS

To simulate numerous extreme events' inundation processes, the reduced-physics model SFINCS (v2.1.1 Dollerup release) was used to efficiently solve the hydrodynamics (Leijnse et al., 2021). SFINCS solves simplified shallow water equations that describe mass and momentum conservation, capturing flood physics while removing computationally expensive terms with minimal impact on large-scale flood behaviour.

The study area was represented on a 400 km² high-resolution grid that covers urban Surabaya and nearby coastal waters, with a 1020 × 707 grid cells at 25-meter resolution and incorporating a 2.5-meter sub-grid to enhance accuracy. Sub-grid tables were generated from elevation, roughness, and river path data to improve the precision of water-flow simulations and achieve higher model accuracy, particularly for smaller drainage channels and urban features. Further details on defining grid resolution are provided in Supplement x A: Grid sensitivity analysis.

Elevation data from a 0.4-meter-resolution DEM captures both inland topography and coastal bathymetry (Figure 4). A horizontally static, plate-fixed reference system was utilized, while the MSL was set as a vertical datum. River inflow points for main rivers entering the model domain (Surabaya River and Wonokromo River) were identified based on vector data of river and urban drainage networks obtained from the Indonesian Geospatial Information Agency (2019), and the corresponding inflows were modeled using HydroMT's river setup function (Eilander et al., 2023). Channel bed elevations were obtained from the elevation model by sampling elevations at vertices along the channel network, while channel widths and Manning's roughness values were uniformly assigned to each segment.

Hydraulic structures were represented using a hybrid approach depending on their scale and influence on the primary flow regime. The major flood control gates located on the primary fluvial networks, specifically the Surabaya, Mas, and Jagir Rivers, were intentionally removed from the DEM. This modification simulates a fully open operational state, assuming that operators

https://doi.org/10.5194/egusphere-2026-4592
Preprint. Discussion started: 20 August 2026

would open gates to maximize the deviation of the river discharge away from the city during flood events. Consequently this allows unhindered upstream propagation of tidal and storm surge dynamics, capturing the maximum extent of the backwater effect within the primary channel network. In contrast, smaller secondary sluice gates and culverts within the urban drainage grid were implicitly captured within the DEM. These structures function as static hydraulic controls/weirs, where flow exchange was determined by the crest height sampled from the terrain data. This representation assumes a passive state for the secondary network, where inter-catchment spillover occurs only when water levels exceed the local topographic barriers.

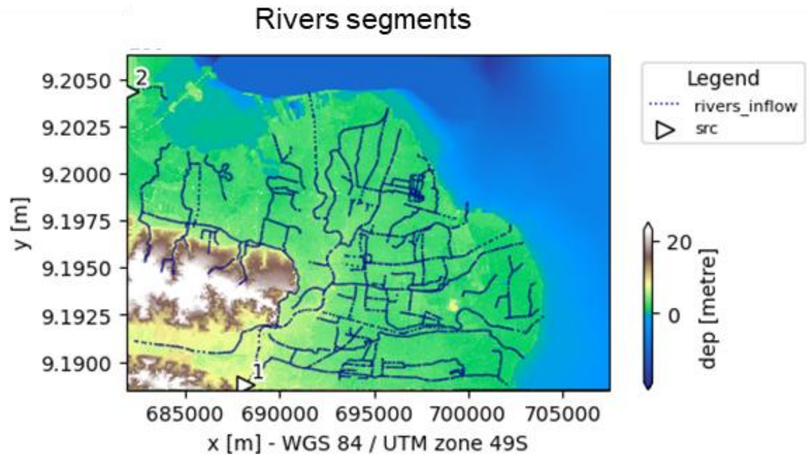

Figure 4: Rivers, drainage, and elevation profile represented in the model region

Surface roughness was represented by spatially varying Manning coefficients derived from the ESA WorldCover map classes (Zanaga et al., 2022). A Manning's roughness coefficient of 0.017 was assigned to rivers and drainage channels based on typical urban channel characteristics. Infiltration processes were simulated using the Soil Conservation Service (SCS) Curve Number (CN) method, adjusted based on Indonesian Ministry of Forestry land cover data (Ministry of Forestry of the Republic of Indonesia, 2019). Antecedent moisture conditions were set to average, and these infiltration parameters were re-projected spatially onto the model grid to estimate runoff. The roughness and topography were assumed to remain unchanged between present day conditions and 2100.

The prepared boundary conditions serve as forcings for 24-hour SFINCS simulation. Forcing data include fixed river inflow discharges, time-varying boundary water levels, and rainfall intensity. A fixed discharge value for the Surabaya River upstream (100 m^3/s) and Lamongan River (10 m^3/s) was selected to account for upper-range conditions during the wet season, representing a conservative model. River inflow and coastal water-level boundary data were provided at 5-minute and 10-minute intervals. Rainfall intensity was modeled with 30-minute temporal resolution over a 6-hour storm duration, assuming spatial uniformity.

https://doi.org/10.5194/egusphere-2026-4592
Preprint. Discussion started: 20 August 2026

3.6 Scenario-based Flood Hazard Assessment

Compound flood hazard assessments were conducted using a scenario-based framework, which allows for evaluating scenarios with the same probability of occurrence but different combinations of driver probabilities. For this purpose, the compound flooding scenarios were associated with a joint return period of 100 years. This framework ensures that different combinations of rainfall and sea-level events are probabilistically consistent (i.e., they have the same compound return period) and that their impacts can be compared equally. Given the statistical independence established during the correlation analysis, which will be described in Section 4.1 Statistical Analysis, the joint return period was calculated as the product of the marginal return periods. The analysis considers scenarios of both single-driver and compound events, all corresponding to a 100-year joint return period. The single-driver scenarios include a 100-year sea-level event (W100) and a 100-year rainfall event (R100). For the R100 scenario, the 100-year rainfall was paired with the HAT. The HAT value was determined by extracting the maximum tidal elevation from the 44-year astronomical tide reanalysis, excluding all meteorological surge residuals (Muis et al., 2022). The HAT used for the R100 boundary was 2.07 meters. The W100 scenario assumes dry conditions (0 mm rainfall) to isolate the coastal flooding footprint. The compound scenarios consist of pairings with lower individual return periods whose joint probability equates to a 100-year event, as detailed in Table 2.

Table 2. Combinations of rainfall and sea-level return periods. The joint return period (100 years) was derived assuming driver independence, justified by the statistical correlation analysis presented in Table 4.

Scenario	Return Period (years)	
	Rainfall	Sea level
W100	none	100
R5W20	5	20
R10W10	10	10
R20W5	20	5
R100	100	HAT

3.7 Impact Metrics

To quantify the flood hazard and the effects of driver interaction, two primary impact metrics were extracted from each simulation: 1) Total inundated area, defined as areas experiencing a flood depth greater than 5 cm, and 2) Maximum water depth across the inundated area. The potential amplification of the flooded area was determined through a spatial analysis in QGIS to identify and quantify the additional area of flooding caused by the interaction of rainfall and extreme sea levels. For each compound scenario (R5W20, R10W10, and R20W5), the resulting inundation map was overlaid with the inundation maps from the single-driver R100 and W100 scenarios. The amplification area was then identified as the flooded region from a compound event that remained dry during the rainfall-only (R100) or coastal-only (W100) simulations. This area represents the spatial extent of flooding exclusively attributable to the interaction between the two drivers. These newly flooded areas were isolated, and their total area was calculated to quantify the amplification magnitude for each compound-event pairing.

https://doi.org/10.5194/egusphere-2026-4592
Preprint. Discussion started: 20 August 2026

In addition to the changes in flood extent, the amplification of flood intensity was analyzed by examining the maximum water depth (*hmax*). For each compound scenario, a pixel-by-pixel ratio was calculated against the corresponding single-driver baselines (R100 and W100) for shared inundated areas:

$$Ratio = 1 - \frac{h_{max,compound}}{h_{max,single}} \quad (1)$$

This calculation was restricted to pixels where $h_{max,single}$ > 5 cm. Pixels where the single driver depth was less than the 5cm threshold, but the compound depth was larger, were classified separately as new flood area of extent amplification. The resulting ratio maps indicate the nature of the interaction:

- Positive ratio: the single-driver event produces larger depths, and compound pairing shows no amplification.
- Negative ratio: the compound interaction creates larger depths than the extreme single driver alone.

To identify the most critical interaction zones, the two resulting ratio maps for each compound scenario were spatially compared. The final flood-depth amplification area was defined as the overlapping region where amplification occurred relative to both the R100 and W100 scenarios (i.e., where both ratio calculations yielded negative values). The proportion of the amplification area relative to the total inundated area of the compound event was calculated to understand the overall contribution of interaction effects to the flood hazard.

3.8 Projection of Future Compound Flood Hazard

The compound flood hazard was extended to project future conditions for the year 2100. This was achieved by modifying the baseline flood drivers (defined in section 3.4) according to two distinct climate scenarios: 1) SSP2-4.5 (intermediate emissions), and 2) SSP5-8.5 (high emissions), based on the framework by Riahi et al. (2017).

The hydraulic model was then re-initialized for all design scenarios (W100, R100, and the compound pairings) using the adjusted boundary conditions. Specifically, the relative sea-level rise increments and rainfall intensification factors detailed on section 3.4 were applied to the boundary inputs. The rest of the simulation setup, including roughness and topography, remained unchanged from the baseline to isolate the climatic influence.

The same impact metrics, total inundated area and flood-depth amplification, were extracted from these future simulations. The present and projected extreme sea levels for design return periods are presented in Table C1.

Finally, the shift in flood frequency was estimated by re-evaluating the joint exceedance probabilities under future conditions. Assuming the statistical independence between drivers remains unchanged, the future joint annual exceedance probability ($P_{J,2100}$) was calculated based on the shifted marginal return periods of the projected rainfall and sea-level distributions:

$$P_{J,2100} = P_{P,2100} \times P_{SL,2100}$$

The result was then converted back to a return period, $T = 1/P_{J,2100}$, to quantify the recurrence interval. This approach isolates the impact of changes in driver magnitude on the recurrence interval of compound events.

https://doi.org/10.5194/egusphere-2026-4592
Preprint. Discussion started: 20 August 2026

4 Results

4.1 Statistical Analysis

(R^2 values between 0.991 and 0.996). The high goodness-of-fit statistics confirm that the exponential tail model is suitable for characterizing the extreme surge and daily rainfall excesses. Return-level estimates were derived from the fitted tail model for surge and rainfall values for different return periods, and summarized in Table 3. The variables' values resulting from this analysis are effectively statistical extrapolation outputs and bounded only by the assumed distribution and data range. However, we acknowledge that in reality, extreme rainfall and storm surge residuals are subject to upper physical boundaries that are not captured by these unconstrained statistical model.

Table 3. Estimated return levels for extreme daily rainfall and storm surge heights in Surabaya (1981 – 2024)

Return Period (years)	Daily rainfall (mm)	Storm surge (m)
1	81.5	0.256
5	111.0	0.299
10	123.6	0.318
20	136.3	0.336
100	165.7	0.379

The Peak Over Threshold was conducted for events exceeding the 95th percentile to explore the correlation between high-quantile rainfall and corresponding storm surge events. The correlation analysis was intentionally conditioned strictly on high-quantile rainfall events. Because the local climate contains a high frequency of dry days, conditioning the analysis on extreme storm surge residuals results in a heavily zero-inflated rainfall vector, which distorts rank-correlation coefficients and misrepresents compounding mechanisms. As presented in Table 4, Kendall's τ values remain strictly below 0.2 across all thresholds, indicating weak to very weak correlations (Higgins, 2004). With the exception of the 99.5% quantile, where a weak positive correlation (τ = 0.1997) registered as statistically significant (p = 0.016), all other thresholds demonstrated no significant dependency ($p > 0.05$). Even at the 99.5% threshold, the magnitude of the correlation remains weak, indicating no substantial physical coupling. Overall, these results demonstrate a statistical independence between rainfall intensity and extreme sea levels in the study area. Consequently, the subsequent analysis will be carried out by independently considering each flooding driver.

https://doi.org/10.5194/egusphere-2026-4592
Preprint. Discussion started: 20 August 2026

Table 4. Statistical correlation between high-quantile rainfall and storm surge residuals. Correlation is quantified using Kendall's τ for paired events occurring within a ± 1-day window across varying percentiles. Statistical significance is assessed at the $p < 0.05$ level.

Rainfall quantile	Kendall's τ	P value	Number of pairs, n
95%	0.0194	0.506	529
97.5%	0.0557	0.147	378
99%	0.0777	0.193	130
99.5%	0.1997	0.016	69
99.9%	-0.0286	0.923	15

4.2 Compound hazard assessment

The nonlinear interaction between coastal and pluvial drivers was measured by focusing on two primary metrics: the increase of flood extent and the increase of flood depth. The overall flood extent for each 100-year joint return period scenario is composed of four distinct components: areas inundated by rainfall-only (R), coastal-only (W), areas flooded by both drivers in their individual scenarios (R∩W), and areas flooded exclusively due to the compound interaction (C), which is defined as the amplification area. Figure 5 provides an overview of the total inundated area and the proportional contribution of each component for all present and future scenarios. Throughout all scenarios in the present climate condition, the total flood extent of approximately 123.8 km² is dominated by two components: rainfall-only (R), which accounts for 44.3% of the area, and the zone of overlap where both individual drivers cause flooding (R∩W), which accounts for about 46.7%. The coastal-only (W) component is smaller, contributing 8.2% of the total flooded area.

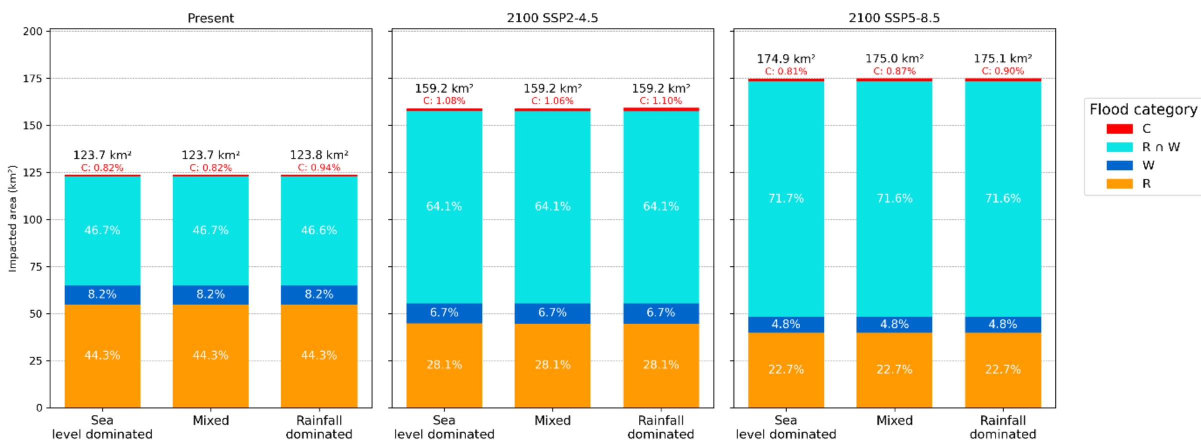

Figure 5: Total inundated area and the proportional contribution of each flood category for present-day, 2100 SSP2-4.5, and 2100 SSP5-8.5 scenarios. The compound flood scenarios are categorized by the dominant driver's return period: coastal dominated (5-year rainfall AND 20-year coastal water level: R5W20), Mixed (10-year rainfall AND 10-year coastal water level: R10W10), and Rainfall dominated (20-year rainfall AND 5-year coastal water level: R20W5). Flood categories are rainfall-only (R), coastal-only (W), overlap between the two drivers (R∩W), and compound (C).

https://doi.org/10.5194/egusphere-2026-4592
Preprint. Discussion started: 20 August 2026

Under the future climate scenarios with a time horizon of 2100, a dramatic shift in flood composition occurs. The total inundated area expands significantly to 159.2 km² (SSP2-4.5) and 175.0 km² (SSP5-8.5). This expansion is driven primarily by the large growth of the overlap zone (R∩W), which accounts for 64.1% and 71.6% of the total flood extent under the SSP2-4.5 and SSP5-8.5 scenarios, respectively. This indicates that future flooding will be characterized by a much larger area influenced simultaneously by coastal and pluvial processes. Consequently, the proportional contributions of rainfall-only (R) and coastal-only (W) areas decrease substantially.

While the amplification area (C) consistently constitutes the smallest portion of the total flood extent, ranging from 0.82% to 1.10% across all scenarios, its importance lies not in its relative size, but in its identity as a newly flooded area. This component represents the direct, nonlinear consequence of driver interaction, creating flood risk in locations that would otherwise remain dry under single-driver conditions. The following sections will focus on detailed spatial and quantitative analysis of the amplification components.

4.2.1 Amplification of flood extent

Under present-day conditions, the amplification of flood extent contributes approximately 1.0 to 1.2 km² of additional flooding. As previously illustrated in Figure 5, the rainfall-dominant scenario (R20W5) produces the largest amplification area (1.2 km^2, 0.94% of total flooded area), while the mixed (R10W10) and sea-level dominant (R5W20) scenarios produce slightly smaller areas of 1 km^2 (0.82% of total flooded area). The spatial distribution of flood extents across scenarios for present climate-change condition is presented in Figure 6. Through these equivalent joint scenarios, we observe that while a high sea level is necessary to generate the initial backwater effect, the larger volume of rainfall may provide the water needed to fill and subsequently spill over from a greater number of local depressions, extending the flood into new areas. This highlights a critical nonlinear interaction where the coastal driver enables the pluvial driver to have a much larger impact than it would in isolation.

https://doi.org/10.5194/egusphere-2026-4592
Preprint. Discussion started: 20 August 2026

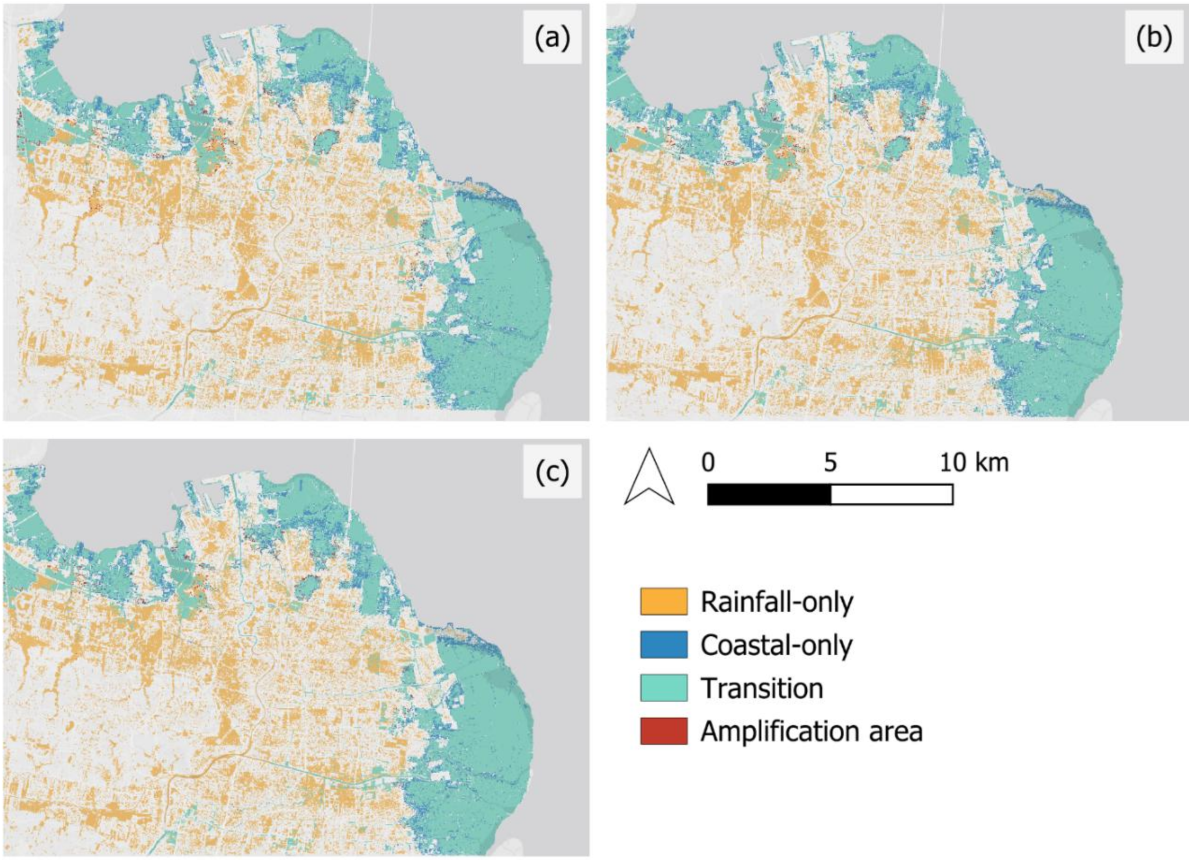

Figure 6: Present-day spatial distribution of flood extents for each category for the rainfall-dominated (R20W5) (a), mixed (R10W10) (b), and coastal-dominated (R5W20) (c) scenarios. Basemap: Esri Light Gray Canvas. Sources: Esri, TomTom, Garmin, NASA, NGA, USGS, METI/NASA | Powered by Esri.

For the expansion of flooded areas, the volume of rainfall runoff is a more critical factor than the magnitude of the coastal water level, provided that the coastal water level is sufficient to obstruct gravity drainage. This relation is demonstrated by the rainfall-dominant scenario (R20W5), which yields the largest amplification area despite having a lower sea level than the mixed or coastal-dominant scenarios (R5W20). The presence of even a moderate coastal water creates a backwater effect that traps runoff. Spatially, these amplification areas are not random. They manifest as many scattered clusters located at the interface between the coastal flood zone and the inland pluvial flood zones (Figure 11). These hotspots are particularly concentrated along the fringes of the drainage canals and rivers within the northern and eastern parts of the city.

https://doi.org/10.5194/egusphere-2026-4592
Preprint. Discussion started: 20 August 2026

4.2.2 Amplification of flood depth

Beyond expanding the flood footprint, the interaction between coastal and pluvial drivers also intensifies the hazard by increasing water depths. The analysis identifies the flood-depth amplification area, defined as the zone where the flood depth under a compound scenario exceeds the depth produced by both the rainfall-only (R100) and the coastal-only (W100) events. These are the locations where the compound hazard is unequivocally more severe than either individual driver acting alone. The delineation of the flood-depth amplification area for the sea level-dominated compound (R5W20) scenario is illustrated as a representative case in Figure 11. To evaluate consistency across all examined joint probabilities, Figure 8 compares the spatial distribution of these depth-amplification areas across all present-day scenarios. The substantial overlap between the scenarios in the figure indicates that the locations of these hotspots are highly consistent across different combinations of rainfall and sea level.

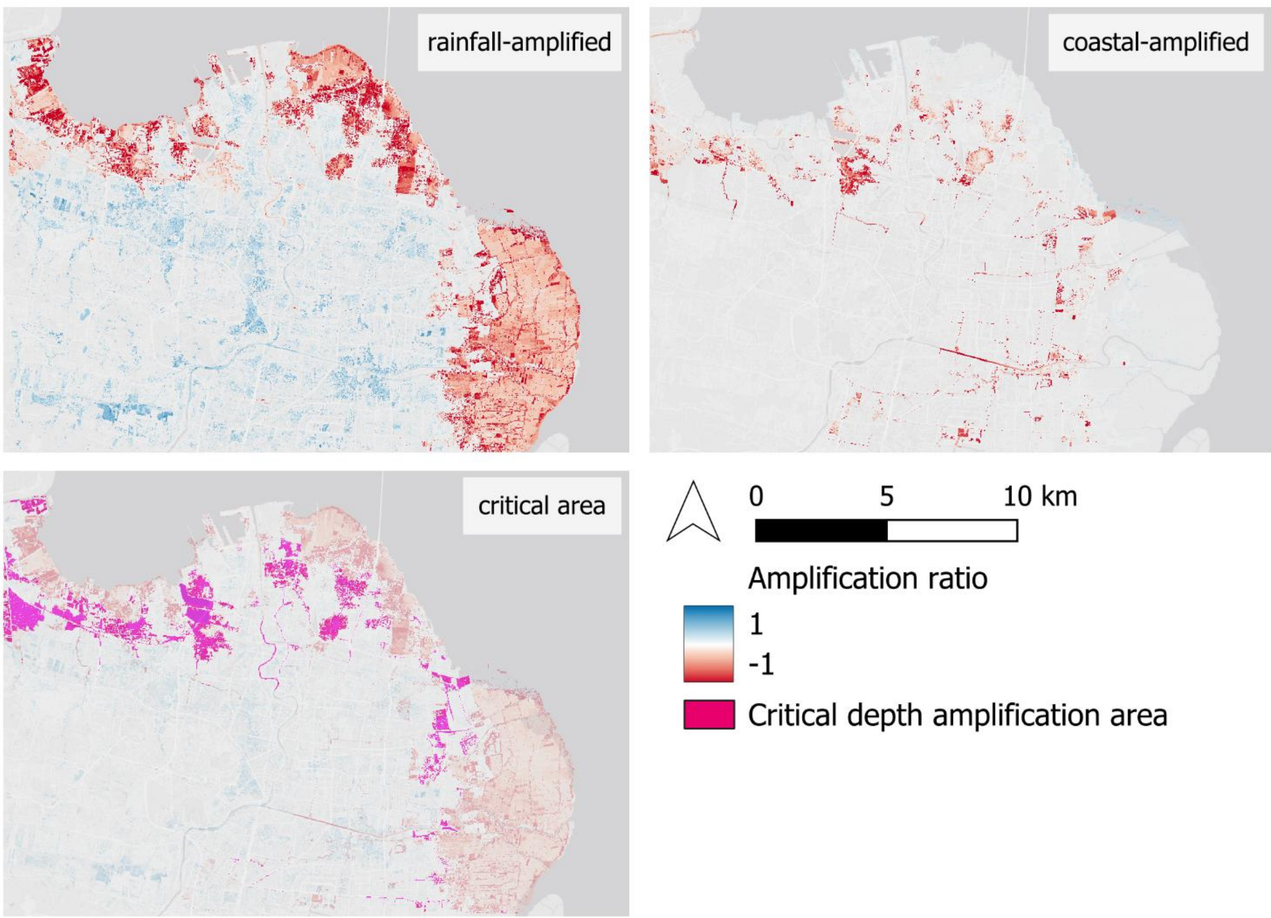

Figure 7: Delineation of the flood-depth amplification area for the coastal-dominated (R5W20) scenario. The final area (bottom panel, magenta) is identified by finding the spatial overlap of zones where the compound depth exceeds the rainfall-only depth (R100) (top-left) and the coastal-only depth (W100) (top-right). Red indicates amplification while blue indicates no amplification. Basemap: Esri Light Gray Canvas. Sources: Esri, TomTom, Garmin, NASA, NGA, USGS, METI/NASA | Powered by Esri.

https://doi.org/10.5194/egusphere-2026-4592
Preprint. Discussion started: 20 August 2026

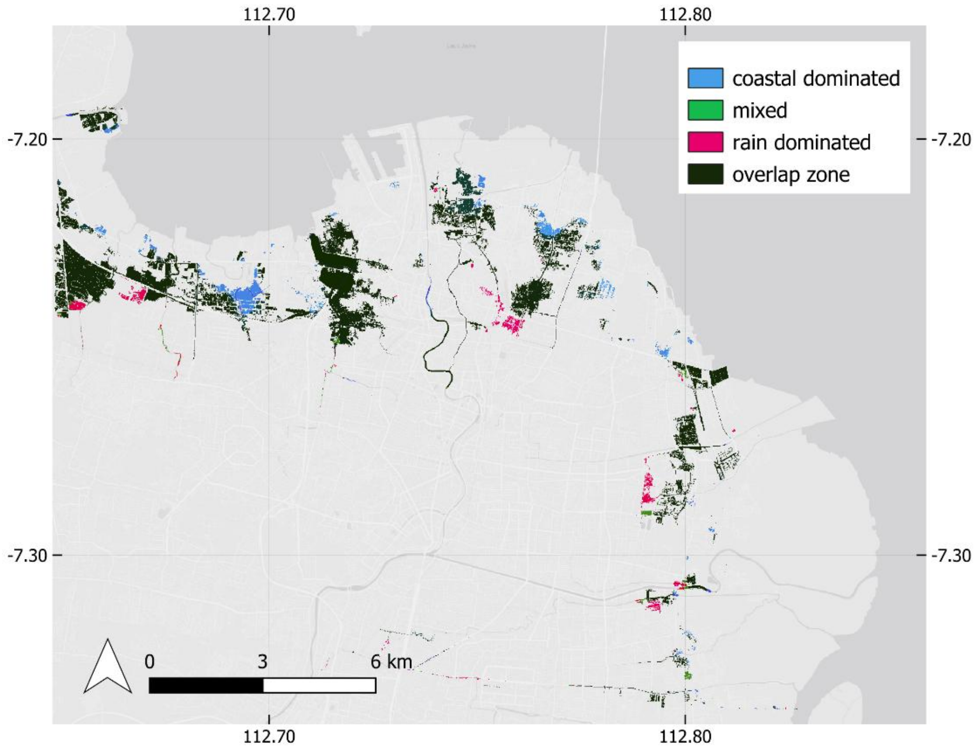

Figure 8: Flood-depth amplification areas under present conditions for the coastal-dominated (R5W20), mixed (R10W10), and rainfall-dominated (R20W5) scenarios. Larger parts of these zones overlap in the black shaded areas. Basemap: Esri Light Gray CanvasSources: Esri, TomTom, Garmin, NASA, NGA, USGS, METI/NASA | Powered by Esri.

As shown in Figure 7, the amplification of flood depth occurs in distinct, localized hotspots rather than across the entire floodplain. A large portion of these areas is concentrated in the northern and western parts of the study area. These zones align with the main drainage channels and low-lying urban areas where the backwater effect from high sea levels severely impedes the discharge of rainwater, causing water to accumulate to greater depths. Smaller, more scattered pockets of depth amplification are also visible in the city's eastern and southern parts. Table 5 summarizes the quantitative results. In contrast to the small area of extent amplification (<1%), the amplification of depth affects a much larger portion of the floodplain.

The coastal-dominated scenario (R5W20) generates the largest flood-depth amplification area at 11.9 km², covering 9.6% of the total inundated area. As rainfall influence increases and sea level influence decreases (moving from scenario R5W20 to scenario R20W5), the flood-depth amplification area decreases slightly. Overall, between 8.7% and 9.6% of the total flooded area experiences unequivocally more severe flooding due to the compound effect.

Under the 2100 climate change scenarios, the flood-depth amplification area is projected to expand dramatically. Table 5 compares the size of this area across the present-day and future scenarios. Under the moderate SSP2-4.5 scenario, the area experiencing depth amplification is projected to more than double, increasing by 124% to 154%. The coastal-dominated scenario continues to produce the largest amplification area (30.2 km²). Under the high-emission SSP5-8.5 scenario, the amplification becomes even more extreme. The area of increased depths triples, with increases of over 200% from the present

https://doi.org/10.5194/egusphere-2026-4592
Preprint. Discussion started: 20 August 2026

for the coastal-dominated and mixed scenarios. The coastal-dominated scenario produces the largest flood-depth amplification area at 36.6 km², followed closely by the mixed scenario at 33.2 km². This finding highlights the critical role of extreme sea-level rise in a high-emission future; its influence on the backwater effect becomes so strong that it greatly amplifies flood depth, resulting in the most severe outcomes.

The spatial distribution of this future hazard is shown in Figure 9 for the SSP2-4.5 and SSP5-8.5 scenarios. A comparison with the present-day conditions (Figure 8) shows a dramatic transformation. The previously localized hotspots are projected to expand and merge into large, contiguous zones of intensified flooding. This effect is most pronounced in the coastal-dominated scenario (R5W20, shown in blue), where the amplification covers a larger area across the northern and western coastal plains.

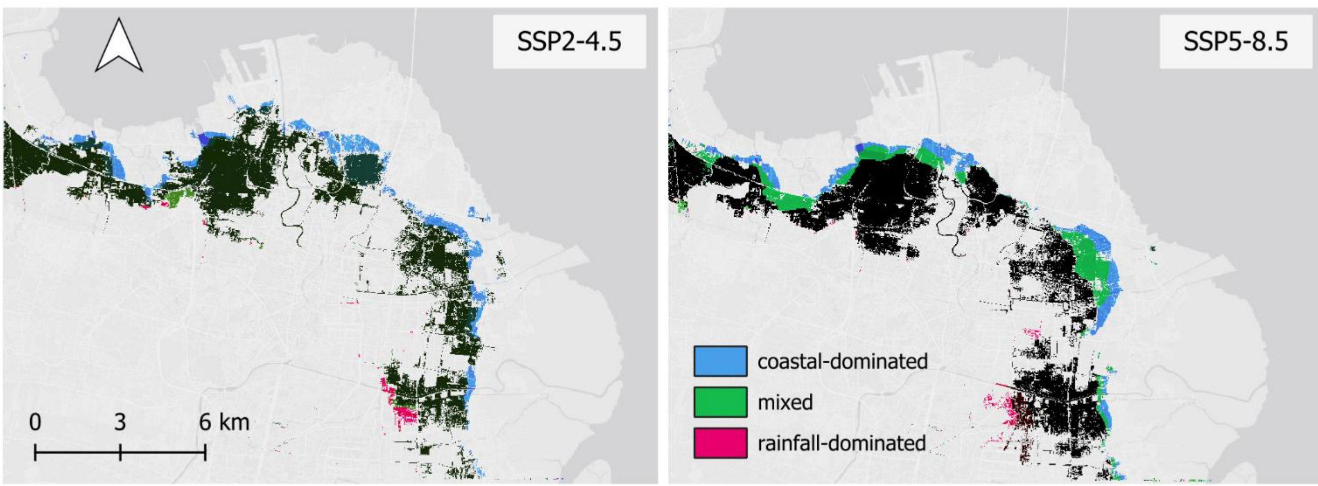

Figure 9: Flood-depth amplification areas by 2100 under SSP2-4.5 (left panel) and SSP5-8.5 (right panel) for the coastal-dominated (R5W20), mixed (R10W10), and rainfall-dominated (R20W5) scenarios . Areas of overlap between scenarios are shown in the black shaded areas. Basemap: Esri Light Gray CanvasSources: Esri, TomTom, Garmin, NASA, NGA, USGS, METI/NASA | Powered by Esri.

Table 5. Flood-depth amplification area for present-day and future climate scenarios

Scenario	Area (km^2)			Proportion of total inundated area (%)		
	Present-day	$2100_{SSP2\text{-}4.5}$	$2100_{SSP5\text{-}8.5}$	Present-day	$2100_{SSP2\text{-}4.5}$	$2100_{SSP5\text{-}8.5}$
Rainfall-dominated	11.9	30.2	36.6	9.6	18.9	20.9
Mixed	10.9	26.5	33.2	8.8	16.6	18.9
Coastal-dominated	10.7	24.0	28.2	8.6	15.1	16.1

Building on the finding that flood depths are amplified under compound scenarios, Table 6 summarises flood hazard statistics, detailing the mean water depth and standard deviation for various flood drivers under present-day conditions and two future climate scenarios for 2100 (SSP2-4.5 and SSP5-8.5). These values are calculated across the inundated area (flood depth > 5 cm) to better understand the flood depth distribution.

https://doi.org/10.5194/egusphere-2026-4592
Preprint. Discussion started: 20 August 2026

A clear trend appears across all types of flooding, from rainfall and compound to coastal floods. Both the average flood depth and the standard deviation consistently increase in future projections, with the highest rise seen under the SSP5-8.5 scenario. Currently, for rainfall flooding, the mean depth is 0.54 m (Std. 0.49). This is expected to rise to 0.7 m (Std. 0.63) under SSP2-4.5, and to 0.84 m (Std. 0.71) under SSP5-8.5. The compound events also show notable increases. For the R5W20 scenario, the mean depth increases from 0.67 m (Std. 0.6) to 0.86 m (Std. 0.72) in SSP2-4.5, reaching 1.03 m (Std. 0.8) in SSP5-8.5. Coastal events have the highest average depth. The current mean depth of 0.91 m (Std. 0.62) rises to 1.04 m (Std. 0.73) in SSP2-4.5, and to 1.21 m (Std. 0.79) in SSP5-8.5. This dual increase indicates that future floods are expected not only to be deeper on average but also to exhibit greater variability across different locations.

However, the domain-wide mean maximum flood depth may appear lower for compound events than for pure coastal events. This difference arises because the pluvial driver extends the inundation area into peripheral zones with shallow water depths. These extensive shallow areas effectively dilute the domain-wide average, masking the severe, localized deepening occurring within the critical backwater zones. Therefore, flood-hazard assessment should consider both spatially explicit depth-difference maps and aggregated summary statistics.

Table 6. Comparison of mean maximum flood depth and standard deviation for various flood drivers under present-day conditions and future climate scenarios for the year 2100.

Driver	Present		2100 SSP2-4.5		2100 SSP5-8.5	
	Mean max. water depth (m)	Std.	Mean max. water depth (m)	Std.	Mean max. water depth (m)	Std.
Rainfall-only (R100)	0.536	0.490	0.702	0.630	0.840	0.705
Rainfall-dominated (R20W5)	0.635	0.578	0.826	0.703	0.993	0.779
Mixed (R10W10)	0.650	0.587	0.840	0.710	1.009	0.785
Coastal-dominated (R5W20)	0.665	0.596	0.856	0.717	1.025	0.791
Coastal-only (W100)	0.912	0.615	1.040	0.730	1.206	0.786

4.3 Frequency increases in flood drivers under future climate conditions

By spatially comparing the projected 2100 flood footprints against the present-day baseline, the analysis quantifies the non-linear amplification of flood hazard intensity driven by the changing climate. The analysis of future recurrence intervals reveals a strong disparity in how climate change affects different flood drivers (Figure 10). The shift in frequency is not uniform across variables.

The shift in the rainfall return periods is moderate. As shown in Figure 10 (left), the present-day 100-year rainfall event in grey shifts to lower return periods under future scenarios, but the magnitude of shift is relatively small. This reflects projected intensification factors of approximately 17-24%, which shorten the recurrence intervals but still keeping these events within the range of relatively rare extremes rather than chronic hazards.

In contrast, the shift in extreme sea levels is disproportionately larger (Figure 10, center). With the projected MSL rise of up to 0.92 m by 2100 (SSP5-8.5), the frequency curve undergoes a substantial shift. Events that are currently considered extreme

https://doi.org/10.5194/egusphere-2026-4592
Preprint. Discussion started: 20 August 2026

(100-year return period) are projected to occur more frequently than once per year (<1-year return period) by 2100. This indicates that MSL rise is likely to be a more dominant contributor to future shifts in extreme sea levels frequency than storm surge anomalies (refer to Vousdoukas et al. 2018).

Consequently, the joint probability of compound events (Figure 10, right) is dominated by the sea-level signal. Despite the modest shift in extreme rainfall frequency, the substantial increase in extreme sea levels considerably shifts the joint probability curve toward lower return-period values. A compound event defined as a 100-year hazard in the present day is projected to recur as frequently as every 2-3 years under SSP2-4.5and SSP5-8.5 . This indicates that future compound flood hazards may not expand drastically in terms of flooded area, but they are expected to occur much more frequently.

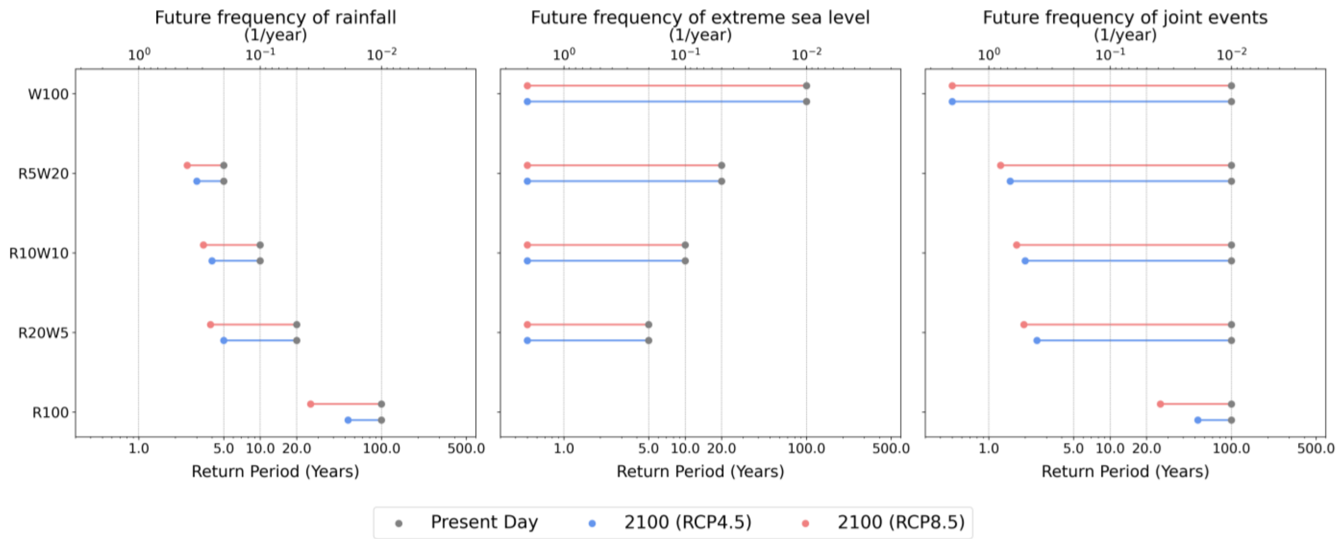

Figure 10: Projected shift in flood recurrence intervals by 2100 relative to present-day conditions (grey) for coastal-only (W100), coastal-dominated (R5W20), mixed (R10W10), rainfall-dominated (R20W5), and rainfall-only (R100) scenarios. The panels display the change in return periods for rainfall (left), extreme sea level (center), and joint compound events (right) under SSP2-4.5 (blue) and SSP5-8.5 (red) emissions scenarios. The substantial leftward shift in the joint probability indicates that a present-day 100 year compound event is projected to recur every 2-3 years by 2100, driven primarily by relative sea-level rise.

5 Discussion

5.1 Statistical independence between drivers

Our statistical analysis revealed a very low correlation ($\tau < 0.2$) between extreme rainfall and storm surge in Surabaya. This finding contrasts with many higher-latitude coastal regions such as North Atlantic or Northwestern Europe, where compound floods are frequently driven by synoptic-scale storms that generate high winds, surges and heavy precipitation simultaneously (Ganguli and Merz, 2019; Lai et al., 2021; Ward et al., 2018).

The independence observed using the flood drivers' reanalysis data in Surabaya can be attributed to its specific meteorological and geographical setting. Located within the Madura Strait, the region is shielded from long-fetch wind generation that limits

https://doi.org/10.5194/egusphere-2026-4592
Preprint. Discussion started: 20 August 2026

the potential for substantial wind-driven surges. Therefore, extreme sea levels in this region are dominated by astronomical tides rather than meteorological storm surges. The storm surge reanalysis record (1981-2024) also indicates a distinct absence of high magnitude surge events typical of extratropical and tropical cyclone-prone regions. Moreover, at approximately -7.25°S, Surabaya lies within the near-equatorial band where the Coriolis force is insufficient to sustain the vorticity required to generate sustained, large-scale wind fields and subsequent storm surges.

Conversely, extreme rainfall is driven by convective processes and the Asian Monsoon system. Extreme rain in Surabaya is primarily produced by ENSO-modulated monsoon circulation and localized convective systems, such as cumulonimbus clouds fueled by warm, humid Java Sea airflows, rather than cyclone-related precipitation (Harjupa and Nakakita, 2025). As a result, Surabaya experiences intense convective rain bursts and short-lived mesoscale rain clusters, which produce high rainfall totals but generate only modest, locally forced winds that have limited ability to generate substantial storm surge over the short Java Sea fetch (Supari et al., 2018; Supari, 2012).

Since the gravitational cycles of the astronomical tides and the atmospheric dynamics of the monsoon rain operate on different timescales, the probability of them coinciding is largely stochastic. Together, these findings support the weak statistical dependence between extreme rainfall and storm surge in the study area.

5.2 Mechanisms of compound interaction

A closer examination of the flood-extent amplification areas reveals a consistent physical mechanism responsible for the creation of these new flood zones across the study area (Figure 13). The process unfolds in several stages. First, the extreme sea level elevates the water stage within the primary river and drainage network. This elevated-water level acts as a hydraulic barrier that reduces or eliminates the pressure gradient required for gravity-based discharge. While the city employs pumping stations to counteract this effect, the current simulation excludes mechanical intervention due to the lack of operational data. If precise data regarding the operational rules and reliability of these flood protection works were available, their inclusion would expectantly demonstrate a localized level of flood mitigation, particularly within the immediate catchments serviced by these active components. Consequently, the results isolate the natural vulnerability of the drainage system, demonstrating that, in the absence of pumping, the drainage capacity is strongly limited by downstream sea-level conditions.

The final and critical stage is the formation of the amplification area. The trapped rainwater accumulates in these local depressions until the water level overtops the subtle topographic divides that would normally contain the flooding. The water then spills into adjacent, slightly higher areas that would not have been flooded by either rainfall or sea level alone. These spillover zones are the red compound areas seen in the maps in Figure 11.

https://doi.org/10.5194/egusphere-2026-4592
Preprint. Discussion started: 20 August 2026

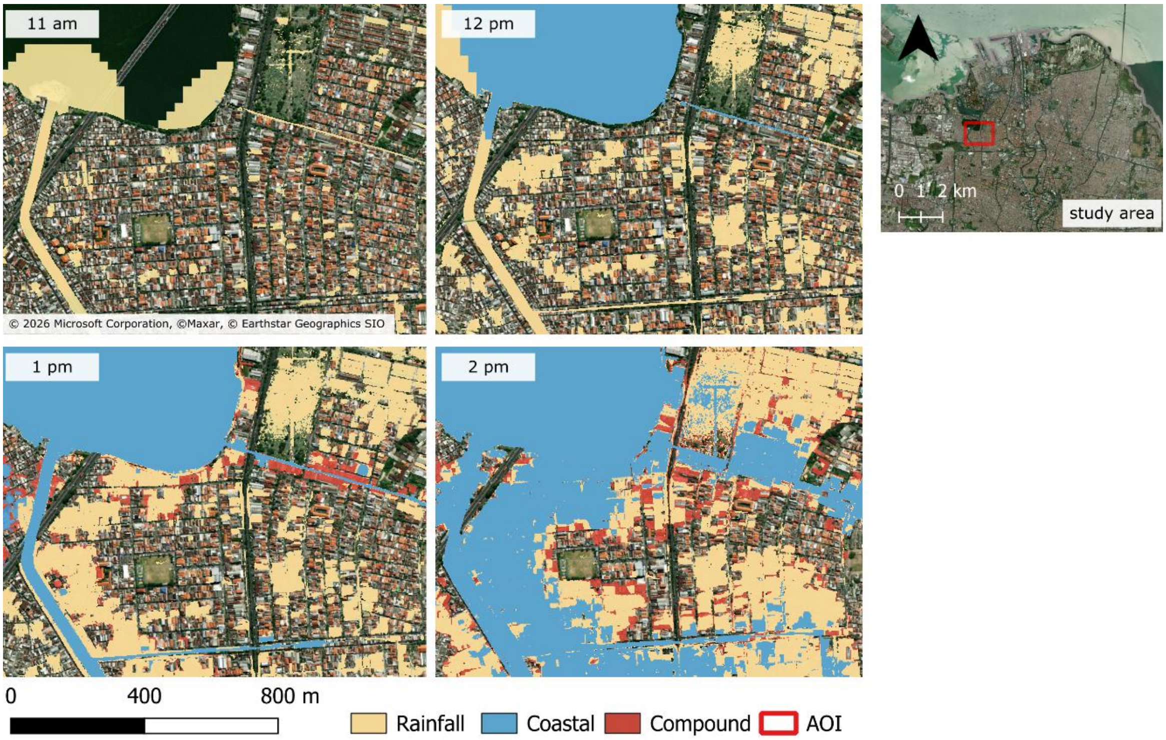

Figure 11: Illustration of the amplification mechanism through hourly snapshots in a detailed view near Bozem Kalianak. The panels demonstrate the process of backwater-induced spillover, where coastal flooding blocks drainage during peak sea level at noon, causing trapped rainwater to accumulate and spill into new areas (red) between 1 pm and 2 pm. Yellow area represents rainfall-only inundation, blue area represents coastal-only inundation, and red area represents amplified inundation that appears in the compound (R20W5) scenario. Microsoft product screen shot(s) reprinted with permission from Microsoft Corporation.

In contrast, flood depth amplification affects a much larger portion of the floodplain (up to 9.6% of the total flood extent under baseline conditions). It intensified the flood depth in areas that are already prone to flooding. Although this intensification is mechanically distinct from the spillover process, it is also primarily driven by the backwater effect, which impedes drainage and causes rainwater that would normally flow through the drainage system to accumulate to greater depths. The comparison between equiprobable scenarios results (Table 6) indicate that, in current conditions, this process is most affected by changes in sea level. To move from this broad floodplain characterization to a localized engineering diagnosis, it is necessary to examine how this systemic depth amplification manifests within individual control structures.

https://doi.org/10.5194/egusphere-2026-4592
Preprint. Discussion started: 20 August 2026

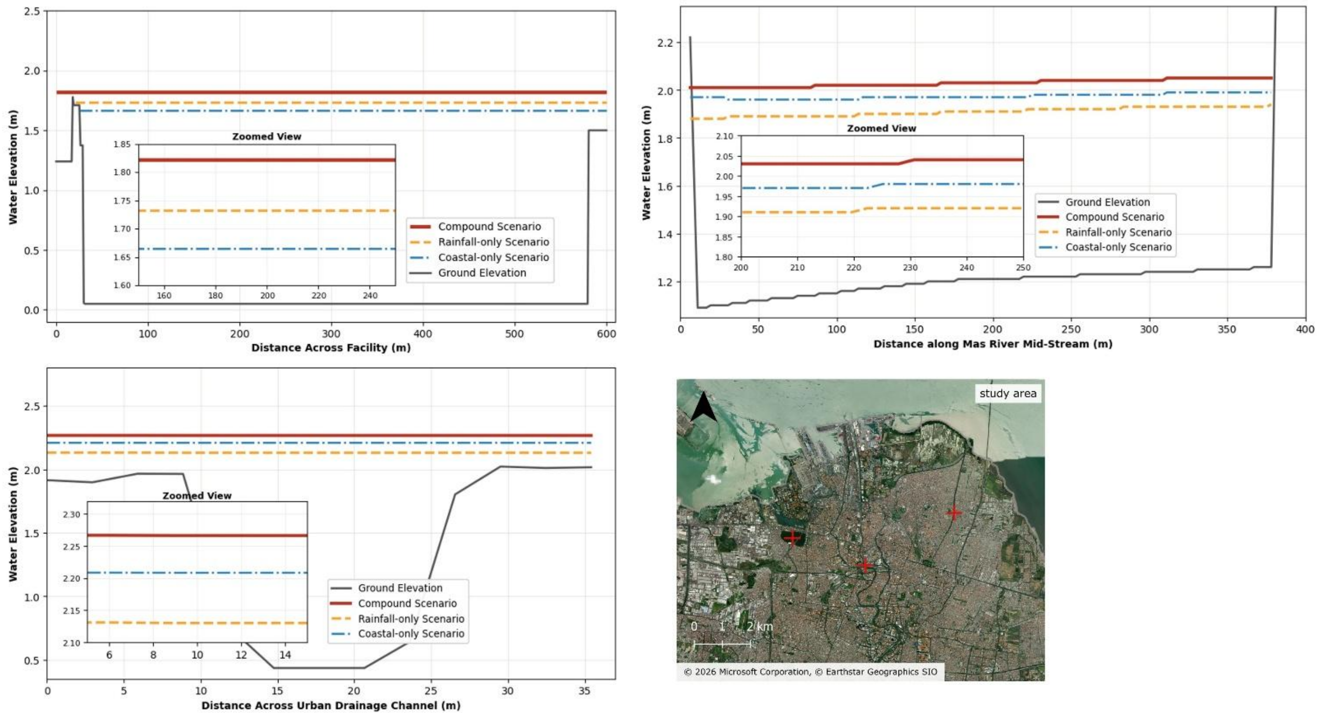

Figure 12: Instantaneous water depth and hydraulic capacity comparison across key urban drainage structures at peak flood (2:00 PM). The profiles illustrate simulated water surface elevations under rainfall-only (R100, orange), coastal-only (W100, blue), and compound (R5W20, red) scenarios. Inset windows display high-magnification views isolating localized centimeter-scale depth differences between scenarios. Panels denote: (a) cross-section of the Boezem Kalianak retention facility, (b) longitudinal profile of the Mas River mid-stream corridor, (c) cross-section of the primary drainage channel, and (d) spatial overview of the study area highlighting the cross-section extraction locations across the urban drainage network. Microsoft product screen shot(s) reprinted with permission from Microsoft Corporation.

To evaluate the spatial and temporal interaction of compounding drivers at the peak inundation period (2:00 PM), the instantaneous water depths across key infrastructure cross-sections under single-driver and joint compound scenarios are compared. To maintain hydrodynamic reliability and mitigate the vertical inaccuracies in high-density urban topographies, samples were restricted to well-defined drainage and retention features. From Figure 12, it is revealed that compound forcing elevates water levels by 5 to 9 cm across the network compared to the highest single-driver events. This range of values represents transition zones characteristics, where the compound water levels are above 5 cm from the single-driver scenario, as described by earlier studies on coastal compound flooding (Bilskie and Hagen, 2018; Eilander et al., 2023; Gori et al., 2020; Shen et al., 2019). The simulated depth amplification also marks a shift in the hydraulic regime. While the coastal-only scenario induces a unidirectional upstream flow from the marine boundary, the compound scenario introduces simultaneous inflows from both the runoff and coastal boundaries. This bidirectional volume accumulation directly compromises downstream tide gates, which typically rely on a positive water level differential to discharge by gravity. Because this baseline simulation reflects a passive system based on strictly by the digital elevation model without active gate or pump regulations, the observed

https://doi.org/10.5194/egusphere-2026-4592
Preprint. Discussion started: 20 August 2026

backup in the urban drainage channel highlights where mechanical pumping infrastructure is fundamentally required to override gravity constraints.

Furthermore, these observations demonstrate the shifts in the frequency and severity of drainage failure and overtopping events, while identifying which local structures are operating at or near maximum capacity. An observed 5-9 cm increase in compound-scenario flood depth in low-lying urban Surabaya-type settings should reasonably be treated as an amplified hydraulic load with operational implications, especially where outfalls, tide gates, pumps, and detention structures already operate close to their design limits. This transition regime highlights the urgency for revisiting both operational rules (e.g., gate timing, pre-event lowering of system storage) and, over the longer term, retrofitting or redesign of drainage and flood-control infrastructure to explicitly account for compound events and rising MSL (Gao et al., 2023; Obara et al., 2025; Yamamoto et al., 2026).

5.3 Driver dominance

The impact of compound flooding is not a uniform intensification; instead, the flood spatial extent and the flood depth are governed by both drivers. The two drivers do not contribute equally to the hazard, instead, they control different aspects of the inundation physics.

The results demonstrate that the expansion of the flood extent is more sensitive to the rainfall component while sea level governs the depth. This finding highlights an important hydraulic decoupling. Rainfall functions primarily as a volumetric driver, as its role is to supply the water required to fill topographic depressions. This explains why the rainfall-dominated scenarios resulted in the widest spatial flood extent. In contrast, sea level functions as the downstream boundary control. Elevating the downstream tailwater sets the minimum potential energy of the entire drainage network. This creates a hydraulic floor that prevents water levels from dropping, regardless of rainfall intensity.

The dominance of the coastal driver is fundamentally linked to the timing of the drainage cycle. Under normal conditions, gravity drainage is possible whenever the river level is higher than the sea level. However, because the modelled storm duration is 6 hours, the effective gravity drainage window is restricted to the low-tide interval of the semi-diurnal cycle. Consequently, elevated coastal boundary condition substantially shortens this drainage window, leaving insufficient time to evacuate the storm runoff before the rising tide re-closes the outlets.

This time-dependent restriction of the drainage window and the spatial transition of driver dominance are explicitly captured through the hourly longitudinal profiles of the Mas River corridor (Figure 13). Under coastal-only forcing (Figure 13a), the incoming water propagates continuously upstream over the 8 km reach, establishing a clear downstream backwater control that elevates the water surface profile. Conversely, the extended pluvial profile (Figure 13b) captures the gravity-driven accumulation of the runoff moving down from the upper catchment. This runoff ultimately pools into a horizontal backwater flow as it meets the elevated tidal boundary. By isolating these independent flow dynamics across space and time, the profiles illustrate that the transition from a gravity-driven flow regime to a tide-locked storage regime downstream is heavily constrained by the semi-diurnal tidal cycle.

https://doi.org/10.5194/egusphere-2026-4592
Preprint. Discussion started: 20 August 2026

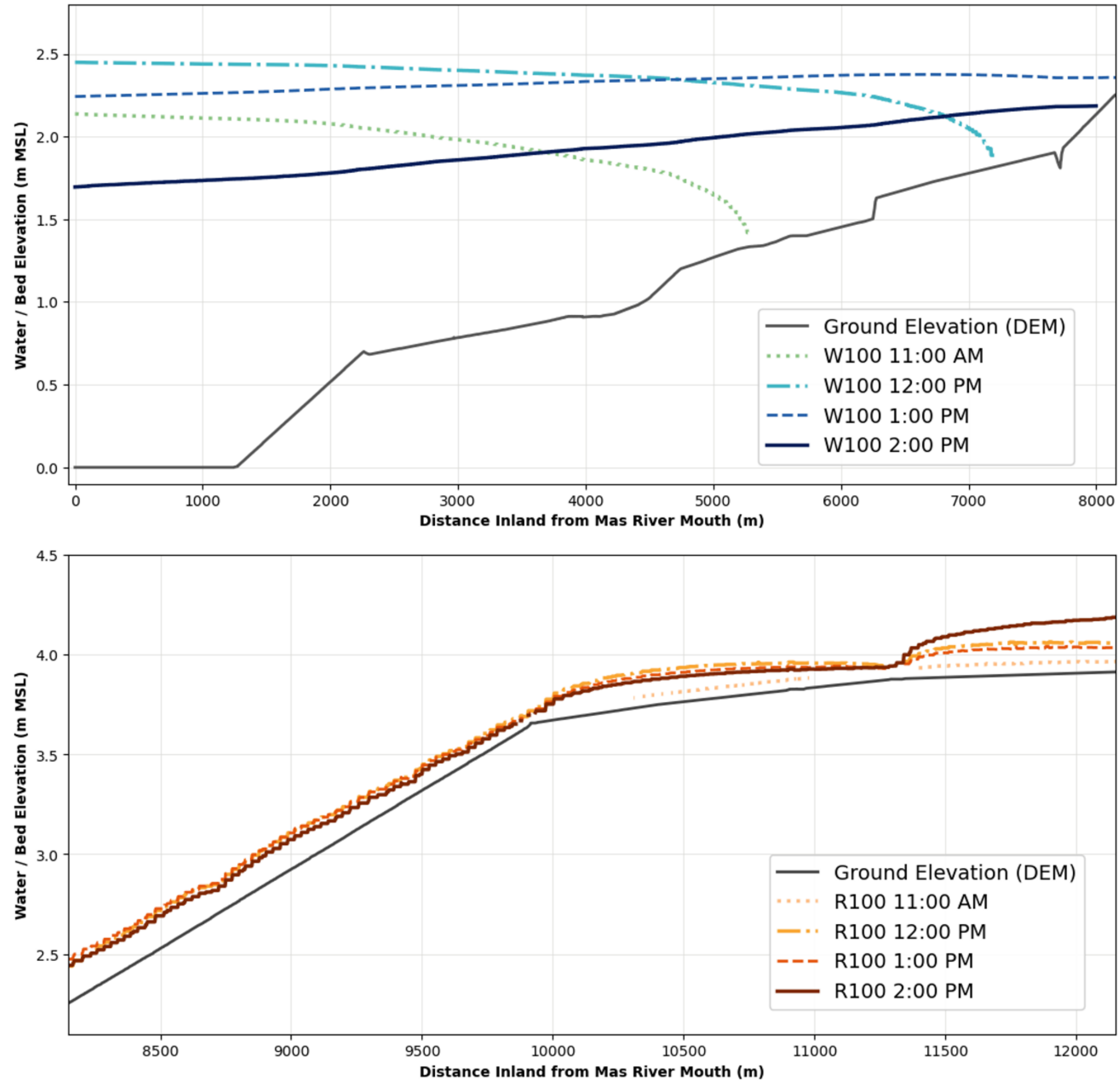

Figure 13: Longitudinal profile comparison of the Mas River drainage corridor demonstrating the spatial-temporal development of flood drivers from 11:00 AM to 2:00 PM. Top panel: coastal-only (W100) scenario water level forcing shows the landward propagation of the backwater wave and an upstream migrating wetting-front along the downstream 8.1 km reach. Lower panel: rainfall-only (R100) scenario pluvial forcing extended 4.2 km into the upper catchment, illustrating friction-dominated gravity flow and a 2-hour hydrograph arrival lag (solid brown line). The grey baseline profile denotes the channel bed elevation.

Under SSP5-8.5 by 2100, the projected sea level will be approximately 0.92 meter higher than the present. The rise of MSL may permanently elevates the downstream boundary above the drainage outlet elevations in Surabaya's flat topography, eliminating the gravity discharge potential. This turns what is currently a temporal drainage constraint into a chronic state, where the outlets will remain partially submerged even at the lowest point of the tidal cycle and transforms the flood hazard from a flow problem into a storage problem.

https://doi.org/10.5194/egusphere-2026-4592
Preprint. Discussion started: 20 August 2026

The asymmetry of driver dominance implies that future adaptation strategies must address the dual nature of the hazard. While inland retention remains effective for managing the rainfall-driven flooding, it is insufficient to mitigate the depth intensification driven by the backwater effect. The results indicate a critical threshold at which passive adaptation (raising infrastructure) becomes economically viable only when paired with active boundary control. Therefore, adaptation strategies may need to shift from a purely increasing conveyance approach to an integrated framework that pairs boundary-control with enhanced internal retention. While active boundary control is required to counteract elevated tailwater, it must be coupled with investments in internal temporary storage and blue-green infrastructure (Harlis and Seo, 2024) to prevent the system from transforming into a functionally closed basin that traps inland runoff.

5.4 Evolution of future hazard

The projection of future hazards highlights a divergence in Surabaya's risk outlook based on different global climate paths. Comparing the moderate (SSP2-4.5) and high emission (SSP5-8.5) scenarios underscores how much the local hazard level depends on global mitigation actions (Riahi et al., 2017).

While both scenarios project an intensification of flooding, the degree of severity diverges considerably. Under the intermediate SSP2-4.5 scenario, the increase in mean maximum flood depth for coastal events is limited to approximately 0.13 m above the baseline. However, this domain wide mean obscures significant spatial variability, the standard deviation increases from roughly 0.62 m in the present day to 0.73 m by 2100, which indicates that localized hazard intensification in vulnerable drainage sectors is substantially higher than the mean shift suggests. While substantial, this increase remains within the theoretical range of conventional engineering defenses, such as raising embankments and upgrading pump capacities (Hinkel et al., 2014).

In contrast, the high-emission SSP5-8.5 scenario increases the mean maximum flood depth by nearly 0.30 m. Similar to the moderate pathway, this average shift is accompanied by an expansion in spatial variance, with the standard deviation rising to 0.79 m, which signals higher localized extremes in the city's lowest-lying zones. This additional hydraulic load represents a tipping point for urban infrastructure. The difference between the two climate pathways corresponds to a massive increase in the volume of water that must be mechanically managed (Sweet and Park, 2014).

The difference between these future flood hazard scenarios may cause an adaptation gap. Under the SSP5-8.5 scenario, the recurrence of the present day 100-year compound event drops to 2–3 years by 2100. This frequency shift implies that without an increase in targeted infrastructure investment, the recovery window between disasters may close completely by the end of the 21st century. Then, the transition from the moderate impacts of SSP2-4.5 to the extreme impacts of SSP5-8.5 may mark the boundary between allowing in-situ adaptation, or having to resort to managed retreat in parts of the city.

Similar patterns of compound flood intensification have been reported for other low-lying tropical cities. In Can Tho, Vietnam, scenario modelling that combines sea-level rise, increased Mekong discharge, enhanced rainfall, and 'business-as-usual' urbanisation indicates substantially greater urban flood extent and depth, particularly when high river levels, tides, and extreme rainfall coincide (Takagi et al., 2014) . Compound fluvial-coastal flood simulations for the wider Mekong delta show that such

https://doi.org/10.5194/egusphere-2026-4592
Preprint. Discussion started: 20 August 2026

co-occurring events inundate larger areas to greater depths and for longer durations in future climates than at present (Wood et al., 2024). In Jakarta, coupled modelling of river discharge and coastal water levels likewise demonstrates that concurrent peaks drive deeper and more widespread urban inundation than single-driver floods, which underscores the importance of compound coastal-fluvial interactions under high-end sea-level rise scenarios (Bennett et al., 2023). Against this regional backdrop, Surabaya's projected increase in flood depth and event frequency under SSP5-8.5 by 2100 is consistent with a broader trend of escalating compound flood hazard across Southeast Asia's coastal cities.

5.5 Study limitations

The accuracy of the flood extent is subject to physical data limitations. The hydraulic modeling relies on a static representation of topography and land use, assuming that roughness coefficients and elevation remain constant over the simulation timelines. While the baseline DEM implicitly reflects the accumulated historical land subsidence up to the data acquisition period, the model does not account for continuous, future geomorphological changes, such as the land subsidence observed in the area or evolving urbanization patterns, that could alter future land elevation, infiltration rates, and surface friction. Furthermore, there is inherent uncertainty in the Digital Elevation Model (DEM) regarding the bathymetry or narrow river channels and drainage canals. If the actual channel depths exceed the resolution capture of the satellite-derived DEM, the model may underestimate the system's conveyance capacity, leading to conservative over-prediction of overbank flow in those specific reaches.

The lack of a data-driven calibration and validation phase also constrains the model's predictive reliability, meaning outputs are indicative rather than precise. However, to evaluate the spatial accuracy of the results, the simulated inundation extents were qualitatively cross-referenced with historical flood documentation from online sources, as detailed in Supplement Appendix B: Model validation.

Beyond the physical properties, the assessment of future hazards relies on specific statistical and temporal simplifications regarding the flood drivers. First, the frequency projections assume that the independence between rainfall and surge remains constant in the future. Although climate change may alter synoptic weather patterns that could induce dependence, the dominant influence of MSL rise suggests that the projected increase in flood frequency is robust regardless of potential shifts in driver correlation (Zscheischler et al., 2018b). Second, the boundary conditions assume a perfect temporal alignment where the peak rainfall intensity coincides exactly with the peak storm surge and HAT. While this phasing creates a robust worst-case stress test, it represents an artificial maximization of the joint hazard.

Finally, a critical assumption in this study is the exclusion of active tide-gate and pumping systems. Although Surabaya utilizes several major structures (i.e. retention basins, gate & pump stations) to force drainage against high tides, operational protocols and pumping capacity data were unavailable for integration into the model. Therefore, the flood extents and depths presented here represent a passive system response as a conservative baseline that effectively simulates scenarios in which pumping capacity is either overwhelmed by extreme inflow or incapacitated by mechanical failure. Because compound flood events can disrupt power supplies and critical infrastructure, analyzing this passive system response provides valuable insights into the city's residual flood risk under defense failure conditions.

https://doi.org/10.5194/egusphere-2026-4592
Preprint. Discussion started: 20 August 2026

Conclusion

This study investigated the compound flood hazard in Surabaya, and focuses on the nonlinear interactions between coastal water levels and rainfall intensity. Through a scenario-based framework and hydrodynamic modeling, the study identified the mechanisms of flood amplification, quantified their impacts under present-day conditions, and projected their evolution under future climate change scenarios. The first part of the study aimed to understand how the dependency between coastal water level and rainfall affects the joint probability of compound flooding. Based on the 44-year historical datasets, the statistical analysis revealed a statistically significant, very low correlation between extreme sea levels and heavy rainfall events in the study area. The occurrence of extreme sea levels is mainly caused by astronomical activity, while heavy rainfall results from atmospheric factors; therefore, there is no common meteorological event for these two events to co-occur. These findings demonstrate that for the current climate, pluvial and coastal extremes in Surabaya are decoupled, supporting the validity of statistical independence in compound hazard assessment.

The second part of the study addressed how the interaction between rainfall intensity and coastal water level amplify the impact of compound flooding. This study identified and quantified two distinct amplification mechanisms: amplification of flood extents and amplification of flood depth. While the spatial extent expansion is modest (approximately 1%), the hydraulic intensity within existing flood zones increases substantially. Compound interaction transforms shallow nuisance flooding into hazardous deep-water zones, affecting 8.6% to 20.9% of the inundated zone which is equivalent to 11.9 - 36.6 km2 across all scenarios. This amplification process was identified as being most sensitive to the sea-level component.

Finally, this study explored that climate change will reshape the flood hazard in Surabaya in two ways. First, increased frequency: The return periods of compound events are projected to compress dramatically. A present-day 1-in-100-year coastal compound flood event is projected to recur as frequently as every 2-3 years under both moderate and high-emission pathways. Second, increased intensity: The severity of flooding will also increase substantially. Mean flood depths will rise across all event types under future scenarios. Although coastal flood produces the highest overall mean depth, compound events generate complex hydraulic interactions that cause severe, localized depth amplification in inland areas due to backwater effects. The total area affected by such critical amplification is projected to triple relative to the present-day conditions. This is driven primarily by sea-level rise, which raises the baseline water stage and exacerbates the backwater effects that intensify pluvial flooding. Consequently, future flood mitigation in Surabaya cannot rely solely on inland drainage capacity; adaptation strategies must balance coastal defense upgrades with enhanced inland retention measures (e.g. temporary water storage basins, blue-green infrastructure) to prevent the entrapment of pluvial runoff when downstream boundary levels block gravity-driven discharge.

However, these projections should be interpreted as a hydrodynamic baseline rather than an exact flood prediction. The current modelling approach isolates the natural system response by excluding the mitigation effects of existing flood control infrastructure (pumping stations and flood gates) and lacks data-driven calibration due to limited historical observations. Consequently, the results characterize the potential magnitude and spatial distribution of flood hazard rather than precise flood

https://doi.org/10.5194/egusphere-2026-4592
Preprint. Discussion started: 20 August 2026

depths. Furthermore, two important local drivers should be incorporated in future research to refine these assessments: upstream fluvial discharge and land subsidence. The latter is particularly urgent for Surabaya, as spatially varying subsidence rates are expected to accelerate relative sea-level rise and alter drainage gradients, likely resulting in flood hazard zones more severe than those projected here. Moving forward, translating these hazard assessments into actionable resilience strategies will require integrating hydrodynamic modelling with socio-economic exposure and vulnerability data to identify the city's high-risk zones.

Appendix A: Grid sensitivity analysis

The maximum flood depth maps produced by the SFINCS simulations form the basis of this analysis. Flood maps in Figure A1 show a relationship between grid resolution and model detail. As illustrated in the plots, inundation patterns became more detailed as grid resolution increased. The 100-m grid produced broad flood extents that failed to capture finer flow pathways. The 50-m grid improved accuracy moderately. The 25-m grid captured localized flood zones more effectively, especially around river mouths, coastal areas, and narrow channels. Slight increases in flood extent with finer grids resulted from improved terrain resolution and smaller flow pathways, indicating coarse grids may underrepresent localized flooding risks in vulnerable areas.

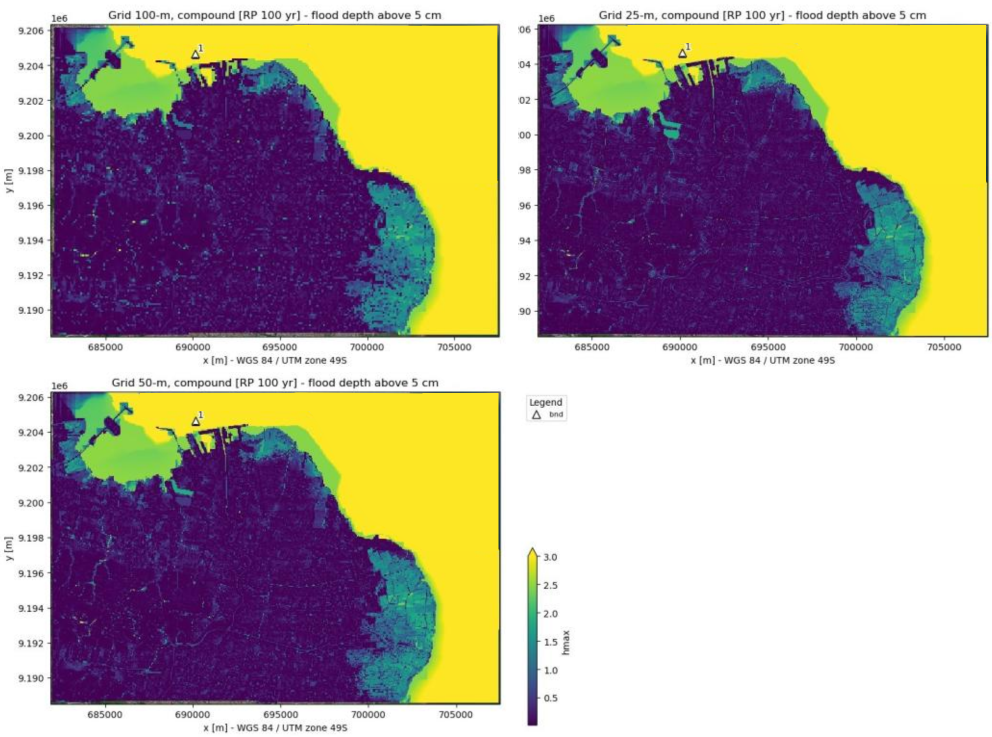

Figure A1: Flood maps of grid size sensitivity tests. An identical compound scenario was simulated with decreasing spatial resolutions of 100 meters (top left), 50 meters (top right), and 25 meters (bottom left).

https://doi.org/10.5194/egusphere-2026-4592
Preprint. Discussion started: 20 August 2026

Model performance was evaluated by running simulations with various parameter adjustments and comparing outcomes to select the best configuration. To assess sensitivity to grid resolution, flood simulations for a 100-year rainfall and sea level scenario used grid sizes of 100 m, 50 m, and 25 m. Subgrid sensitivity testing on the 25-m grid refined spatial accuracy. The 25-m grid was chosen to adequately resolve key hydrodynamic features like narrow drainage channels and small embankments.

Appendix B: Model validation

Model accuracy was assessed by simulating four historical flood events in Surabaya between 2021-2024 and comparing results to documented records. One compound flood on February 6th, 2024, was caused by rainfall and high tides. The other three, from July 4th, 2023; May 19th, 2022; and May 27th, 2021, were coastal floods driven mainly by sea level. Due to lack of in-situ data and satellite images, validation relied on news videos, photos, and social media footage to confirm inundation and estimate flood depths based on features like curbs, walls, vehicles, and pedestrians, especially in neighborhoods like Tambak Dalam Baru, Tambak Pring, Kalianak Timur, Nambangan, and Tanjung Perak Port Access Road.
Four historical flood events were selected as validation cases to evaluate the model's ability to simulate real-world flood scenarios. These events span compound and coastal flood types in Surabaya between 2021 and 2024. One compound flood event on February 6th, 2024, was driven by both intense rainfall and high tidal levels. The other three cases from July 4th, 2023, May 19th, 2022, and May 27th, 2021 were classified as coastal flood events, where sea level was the primary flood driver.
The February 2024 event was modeled using rainfall data from the national meteorological agency (BMKG), accompanied by a sub-daily pattern found in GPM IMERG and corresponding sea level observations recorded at the Surabaya Maritime Station. The SFINCS model was configured to reflect these compound forcing conditions. For the coastal events, simulations were forced only by the observed sea level variations without any rainfall input. The input boundary conditions for the four validation events are displayed, detailing the combined rainfall and sea level drivers for the compound event (Figure B1:) and the sea level-only drivers for the coastal events (Figure B2).

https://doi.org/10.5194/egusphere-2026-4592
Preprint. Discussion started: 20 August 2026

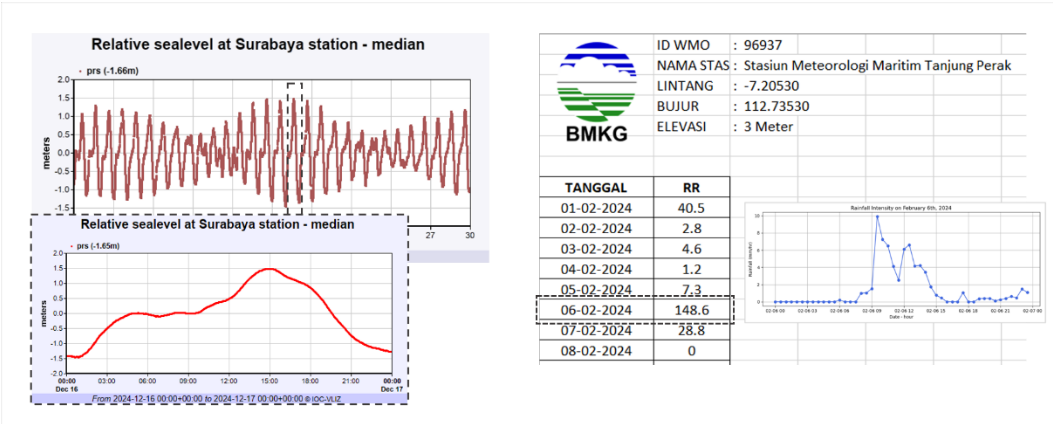

Figure B1: Flood drivers for the compound flood validation event on February 6th, 2024. The figure shows the two concurrent drivers used as model input: the observed sea level time series at the 'sura' tide station (left) and the corresponding rainfall data, including the total depth and temporal distribution (hyetograph), derived from Precipitation Processing System (PPS) at NASA GSFC (2023, right).

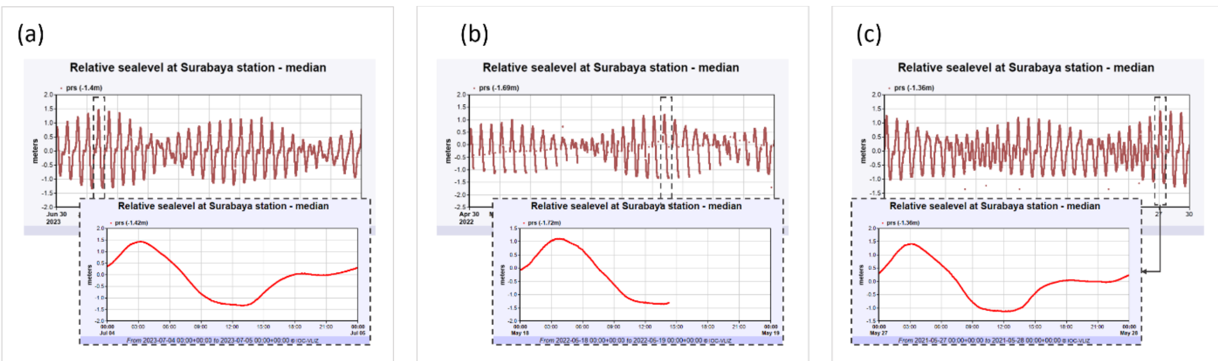

Figure B2: Observed sea level as the primary flood driver for the three coastal flood validation events. The panels show the historical sea level time series used as the sole boundary condition for simulating the coastal-only floods. The events shown are from (a) July 4th, 2023; (b) May 19th, 2022, containing parts of unrecorded water level; and (c) May 27th, 2021.

In the compound flood case of February 6th, 2024, the model successfully reproduced observed flooding conditions in both Tambak Dalam Baru and Tambak Pring, with water depths and flood extent aligning well with visual evidence captured during the event (Figure B3). However, in the three coastal flood cases, the model underestimated inundation at the observed points. While the footages documented flooding in Kalianak Timur, Nambangan, and the Tanjung Perak Port access road, the model showed no inundation in these locations. This discrepancy is attributed to the quality of the input topography data, which lacks the necessary detail to represent fine-scale hydraulic controls in the dense urban landscape.

https://doi.org/10.5194/egusphere-2026-4592
Preprint. Discussion started: 20 August 2026

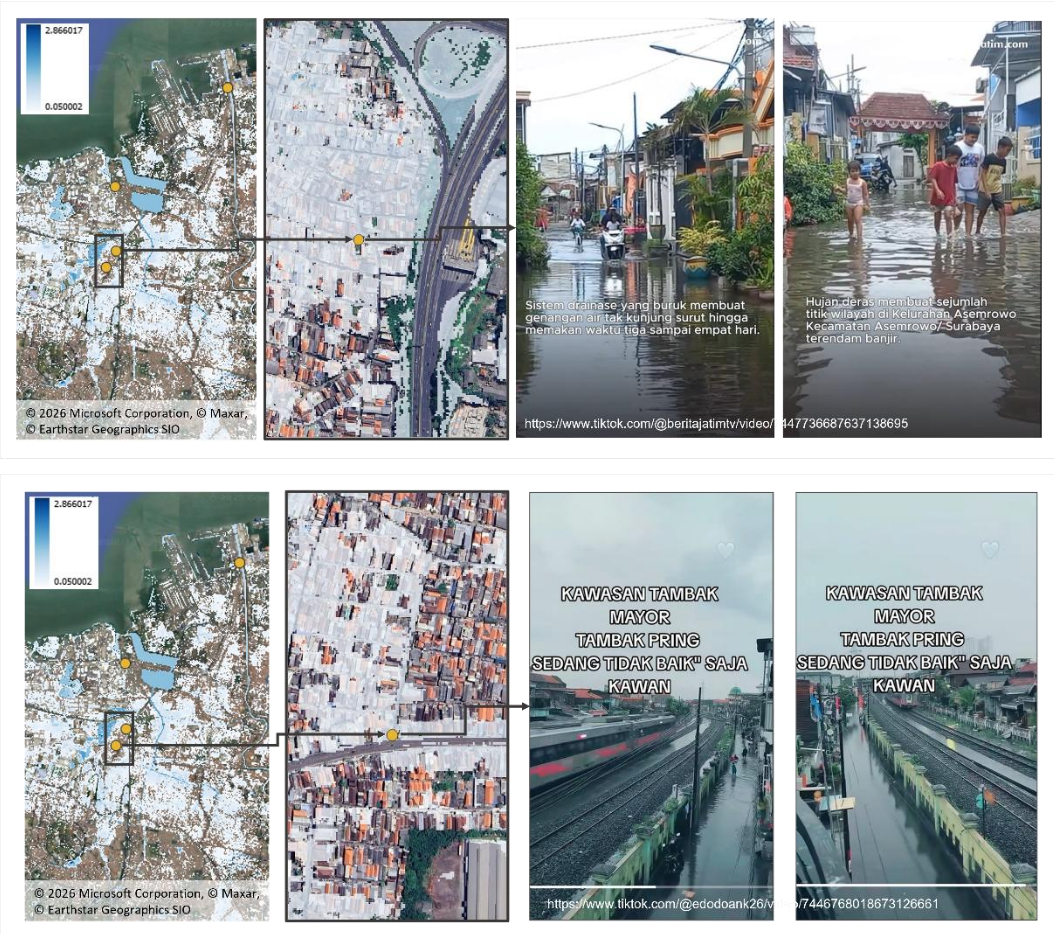

700 **Figure B3: Model validation results for a flood event on 6 February 2024. The simulated inundation maps (left panels), generated using the SFINCS model with rainfall and sea level forcing, are qualitatively compared with photographic evidence of actual flooding (right panels). The comparison is displayed for two locations marked with yellow circles: Tambak Dalam Baru (top row) and Tambak Pring (bottom row). Source: Screenshot from a TikTok video by @beritajatimtv, https://www.tiktok.com/@beritajatimtv/video/7447736687637138695, accessed on 5th April 2025, © @beritajatimtv; Screenshot**
705 **from a TikTok video by @edodoank26, https://www.tiktok.com/@edodoank26/video/7446768018673126661 accessed on 5th April 2025, © @edodoank26. Aerial imagery courtesy of Microsoft Corporation. Microsoft product screen shot(s) reprinted with permission from Microsoft Corporation.**

https://doi.org/10.5194/egusphere-2026-4592
Preprint. Discussion started: 20 August 2026

Appendix C: Present and projected extreme sea levels for design return periods

Table C1. Projected extreme storms and sea levels for the present-day scenarios and projections in 2100

Return Period (years)	6-hours design storm intensity (mm)			Extreme sea level (m)		
	Present	$2100_{SSP2-4.5}$	$2100_{SSP5-8.5}$	Present	$2100_{SSP2-4.5}$	$2100_{SSP5-8.5}$
1	69.3	81.4	85.7	2.328	2.900	3.245
5	92.5	108.6	114.3	2.370	2.942	3.288
10	102.2	120.0	126.3	2.389	2.961	3.307
20	111.7	131.2	138.1	2.408	2.980	3.325
100	133.3	156.6	164.8	2.450	3.022	3.368

Code and data availability

The source code and Python scripts for data analysis and figure generation are hosted on GitHub at https://github.com/agustiaarum/sfincs-surabaya. The repository is currently restricted for peer-review purposes and will be made fully open access upon the formal publication of this manuscript.

Authors contributions

AL, JR, KN, and AD conceptualized the research goals and methodology. AL developed the model code, performed the simulations, and applied the formal analysis with supervision from JR, KN, and AD. AL prepared the manuscript with contributions from all co-authors.

Competing interests

All authors declare no competing interests in this study.

Acknowledgements

References

Agency for Meteorology, Climatology, and Geophysics: Waspada pasang air laut maksimum berlaku mulai tgl 1-5 September yang terjadi di wilayah Surabaya Barat termasuk Gresik, 2024.

Anjasmara, I. M., Yulyta, S. A., and Taufik, M.: Application of Time Series InSAR (SBAS) Method using Sentinel-1A Data for Land Subsidence Detection in Surabaya City, Int. J. Adv. Sci. Eng. Inf. Technol., 10, 191–197, https://doi.org/10.18517/ijaseit.10.1.6749, 2020.

Ardha, M., Khomarudin, M. R., Pranowo, W. S., Chulafak, G. A., Yudhatama, D., Mujio, and Pravitasari, S.: Spatial information on the rate of subsidence in North Coastal Area of Java and the estimation of inundation in 2031, IOP Conf. Ser.: Earth Environ. Sci., 1109, 012022, https://doi.org/10.1088/1755-1315/1109/1/012022, 2022.

Bennett, W. G., Karunarathna, H., Xuan, Y., Kusuma, M. S. B., Farid, M., Kuntoro, A. A., Rahayu, H. P., Kombaitan, B., Septiadi, D., Kesuma, T. N. A., Haigh, R., and Amaratunga, D.: Modelling compound flooding: a case study from Jakarta, Indonesia, Nat Hazards, 118, 277–305, https://doi.org/10.1007/s11069-023-06001-1, 2023.

Bilskie, M. V. and Hagen, S. C.: Defining Flood Zone Transitions in Low-Gradient Coastal Regions, Geophysical Research Letters, 45, 2761–2770, https://doi.org/10.1002/2018GL077524, 2018.

Brotowiryatmo, S. H.: REVIEW OF RAINFALL HOURLY DISTRIBUTION ON THE ISLAND OF JAVA, Journal of the Civil Engineering Forum, 2, 145, https://doi.org/10.22146/jcef.26479, 2016.

Damayanti, A.: Analisis Dampak Perubahan Iklim Berdasarkan Kenaikan Muka Air Laut terhadap Wilayah Kota Surabaya, Master Thesis, Institut Teknologi Sepuluh November, Surabaya, 118 pp., 2016.

Eilander, D., Couasnon, A., Leijnse, T., Ikeuchi, H., Yamazaki, D., Muis, S., Dullaart, J., Haag, A., Winsemius, H. C., and Ward, P. J.: A globally applicable framework for compound flood hazard modeling, Nat. Hazards Earth Syst. Sci., 23, 823–846, https://doi.org/10.5194/nhess-23-823-2023, 2023.

Fitriana, D., Patria, M. P., and Kusratmoko, E.: Karakteristik Pasang Surut Surabaya Diamati Selama 5 Tahun (2015-2020), JGISE, 5, 1, https://doi.org/10.22146/jgise.72856, 2022.

Ganguli, P. and Merz, B.: Trends in Compound Flooding in Northwestern Europe During 1901–2014, Geophysical Research Letters, 46, 10810–10820, https://doi.org/10.1029/2019GL084220, 2019.

Gao, L., Du, H., Huang, H., Zhang, L., and Zhang, P.: Modelling the compound floods upon combined rainfall and storm surge events in a low-lying coastal city, Journal of Hydrology, 627, 130476, https://doi.org/10.1016/j.jhydrol.2023.130476, 2023.

Gori, A., Lin, N., and Xi, D.: Tropical Cyclone Compound Flood Hazard Assessment: From Investigating Drivers to Quantifying Extreme Water Levels, Earth's Future, 8, e2020EF001660, https://doi.org/10.1029/2020EF001660, 2020.

Harjupa, W. and Nakakita, E.: Investigation and future projections of warm rain during the winter monsoon in the Western Java Sea, Indonesia, Front. Clim., 7, 1581382, https://doi.org/10.3389/fclim.2025.1581382, 2025.

Harlis, T. A. and Seo, S. B.: Land suitability analysis for blue-green infrastructure implementation in an urban stormwater management system in Surabaya, Indonesia, Water Science & Technology, 90, 1501–1519, https://doi.org/10.2166/wst.2024.265, 2024.

Higgins, J. J.: An introduction to modern nonparametric statistics, Brooks/Cole Pacific Grove, CA, 2004.

https://doi.org/10.5194/egusphere-2026-4592
Preprint. Discussion started: 20 August 2026

Indonesian Agency for Meteorology, Climatology, and Geophysics: DATA ONLINE - DIREKTORAT DATA DAN KOMPUTASI - BMKG, 2025.

Intergovernmental Panel On Climate Change (Ipcc): Climate Change 2021 – The Physical Science Basis: Working Group I Contribution to the Sixth Assessment Report of the Intergovernmental Panel on Climate Change, 1st ed., Cambridge University Press, https://doi.org/10.1017/9781009157896, 2023.

Jalili Pirani, F. and Najafi, M. R.: Recent Trends in Individual and Multivariate Compound Flood Drivers in Canada's Coasts, Water Resources Research, 56, e2020WR027785, https://doi.org/10.1029/2020WR027785, 2020.

Khansa, P., Sofiyah, E. S., and Suryawan, I. W. K.: Determination of Rain Intensity Based on Rain Characteristics Observed from Rain Observation Stations Around South Jakarta, JACEE, 3, 94, https://doi.org/10.30659/jacee.3.2.106-115, 2020.

Kurniadi, A., Weller, E., Salmond, J., and Aldrian, E.: Future projections of extreme rainfall events in Indonesia, Intl Journal of Climatology, 44, 160–182, https://doi.org/10.1002/joc.8321, 2024.

Lai, Y., Li, J., Gu, X., Liu, C., and Chen, Y. D.: Global compound floods from precipitation and storm surge: Hazards and the roles of cyclones, Journal of Climate, 1–55, https://doi.org/10.1175/JCLI-D-21-0050.1, 2021.

Leijnse, T., Van Ormondt, M., Nederhoff, K., and Van Dongeren, A.: Modeling compound flooding in coastal systems using a computationally efficient reduced-physics solver: Including fluvial, pluvial, tidal, wind- and wave-driven processes, Coastal Engineering, 163, 103796, https://doi.org/10.1016/j.coastaleng.2020.103796, 2021.

Ministry of Forestry of the Republic of Indonesia: Indonesia Land Cover, 2019.

Sanne Muis, Maialen Irazoqui Apecechea, José Antonio Álvarez, Martin Verlaan, Kun Yan, Job Dullaart, Jeroen Aerts, Trang Duong, Rosh Ranasinghe, Dewi le Bars, Rein Haarsma, Malcolm Roberts, (2022): Global sea level change time series from 1950 to 2050 derived from reanalysis and high resolution CMIP6 climate projections. Copernicus Climate Change Service (C3S) Climate Data Store (CDS). DOI: 10.24381/cds.a6d42d60 (Accessed on 09-01-2025)

Nayadiah, E.: Analysis and Evaluation of Urban Drainage and Flood Protection Problems in Surabaya, Case Study: East Surabaya, MSc Thesis, UNESCO-IHE Institute for Water Education and Sriwijaya University, Delft, 139 pp., 2011.

Nicholls, R. J., Lincke, D., Hinkel, J., Brown, S., Vafeidis, A. T., Meyssignac, B., Hanson, S. E., Merkens, J.-L., and Fang, J.: A global analysis of subsidence, relative sea-level change and coastal flood exposure, Nat. Clim. Chang., 11, 338–342, https://doi.org/10.1038/s41558-021-00993-z, 2021.

Obara, C., Fletcher, C. H., Habel, S., McDonald, K., and Yamamoto, K.: Drainage failure and associated urban impacts under combined sea-level rise and precipitation scenarios, Sci Rep, 15, 23436, https://doi.org/10.1038/s41598-025-07332-8, 2025.

Pamungkas, A. and Purwitaningsih, S.: Is Surabaya being planned as a low-risk city?: A case study on the effect of urban spatial plans in the Kedurus catchment area on flash flood risk reduction in Surabaya , IRSPSD International, 9, 78–92, https://doi.org/10.14246/irspsda.9.1_78, 2021.

Patricola, C. M. and Wehner, M. F.: Anthropogenic influences on major tropical cyclone events, Nature, 563, 339–346, https://doi.org/10.1038/s41586-018-0673-2, 2018.

Pineau-Guillou, L., Delouis, J., and Chapron, B.: Characteristics of Storm Surge Events Along the North-East Atlantic Coasts, JGR Oceans, 128, e2022JC019493, https://doi.org/10.1029/2022JC019493, 2023.

Prawira, M. and Pamungkas, A.: Mitigasi Kawasan Rawan Banjir Rob di Kawasan Pantai Utara Surabaya, Jurnal Teknik ITS, 3, 160–165, https://doi.org/DOI:%2010.12962/j23373539.v3i2.7252, 2014.

Precipitation Processing System (PPS) at NASA GSFC: GPM IMERG Final Precipitation L3 Half Hourly 0.1 degree x 0.1 degree V07, https://doi.org/10.5067/GPM/IMERG/3B-HH/07, 2023.

Riahi, K., Van Vuuren, D. P., Kriegler, E., Edmonds, J., O'Neill, B. C., Fujimori, S., Bauer, N., Calvin, K., Dellink, R., Fricko, O., Lutz, W., Popp, A., Cuaresma, J. C., Kc, S., Leimbach, M., Jiang, L., Kram, T., Rao, S., Emmerling, J., Ebi, K., Hasegawa, T., Havlik, P., Humpenöder, F., Da Silva, L. A., Smith, S., Stehfest, E., Bosetti, V., Eom, J., Gernaat, D., Masui, T., Rogelj, J., Strefler, J., Drouet, L., Krey, V., Luderer, G., Harmsen, M., Takahashi, K., Baumstark, L., Doelman, J. C., Kainuma, M., Klimont, Z., Marangoni, G., Lotze-Campen, H., Obersteiner, M., Tabeau, A., and Tavoni, M.: The Shared Socioeconomic Pathways and their energy, land use, and greenhouse gas emissions implications: An overview, Global Environmental Change, 42, 153–168, https://doi.org/10.1016/j.gloenvcha.2016.05.009, 2017.

Riastama, C. N., Anjasmara, I. M., and Maulida, P.: Monitoring Land Subsidence and its Effect on Surabaya Coastal Inundation by Utilizing GPS Campaigns Data, IOP Conf. Ser.: Earth Environ. Sci., 1127, 012002, https://doi.org/10.1088/1755-1315/1127/1/012002, 2023.

Safitri, D. A., Saves, F., Alina, A. N., Bespalova, L. A., and Dhani, N. Q.: Utilization of Geographic Information System for Monitoring Flood Disaster Hazards in Surabaya, Geoinformation Technologies And Space Monitoring, https://doi.org/10.23885/2500-123x, 2024.

Santiago-Collazo, F. L., Bilskie, M. V., and Hagen, S. C.: A comprehensive review of compound inundation models in low-gradient coastal watersheds, Environmental Modelling & Software, 119, 166–181, https://doi.org/10.1016/j.envsoft.2019.06.002, 2019.

Savitri, Y. R., Kakimoto, R., Begum, R. A., Anwar, N., Wardoyo, W., Suryani, E., Graduate School of Science and Technology, Kumamoto University 2-39-1 Kurokami, Chuo-ku, Kumamoto, Kumamoto 860-8555, Japan, Department of Civil Engineering, Institut Teknologi Sepuluh Nopember, Jawa Timur, Indonesia, Faculty of Advanced Science and Technology, Kumamoto University, Kumamoto, Japan, Centre for Corporate Sustainability and Environmental Finance, Macquarie University, New South Wales, Australia, and Department of Information System, Institut Teknologi Sepuluh Nopember, Jawa Timur, Indonesia: The Application of AHP to Determine the Priority Drainage System on Flood Mitigation in Surabaya – Indonesia, JDR, 17, 431–443, https://doi.org/10.20965/jdr.2022.p0431, 2022.

Shen, Y., Morsy, M. M., Huxley, C., Tahvildari, N., and Goodall, J. L.: Flood risk assessment and increased resilience for coastal urban watersheds under the combined impact of storm tide and heavy rainfall, Journal of Hydrology, 579, 124159, https://doi.org/10.1016/j.jhydrol.2019.124159, 2019.

Sulma, S., Kusratmoko, E., and Saraswati, R.: COASTAL PHYSICAL VULNERABILITY OF SURABAYA AND ITS SURROUNDING AREA TO SEA LEVEL RISE, MST, 16, https://doi.org/10.7454/mst.v16i2.1516, 2013.

Supari, Tangang, F., Salimun, E., Aldrian, E., Sopaheluwakan, A., and Juneng, L.: ENSO modulation of seasonal rainfall and extremes in Indonesia, Clim Dyn, 51, 2559–2580, https://doi.org/10.1007/s00382-017-4028-8, 2018.

Supari, S.: Spatiotemporal Characteristics of Extreme Rainfall Events over Java Island, Indonesia, Case: East Java Province, Thesis, Gadjah Mada University, University of Twente, 170 pp., 2012.

Susetyo, C.: Urban Flood Management in Surabaya City, MSc Thesis, International Institute for Geo-Information Science and Earth Observation, Enschede, 2008.

https://doi.org/10.5194/egusphere-2026-4592
Preprint. Discussion started: 20 August 2026

Sweet, W. V. and Park, J.: From the extreme to the mean: Acceleration and tipping points of coastal inundation from sea level rise, Earth's Future, 2, 579–600, https://doi.org/10.1002/2014EF000272, 2014.

Takagi, H., Ty, T. V., and Thao, N. D.: Investigation on Floods in Can Tho City, in: Coastal Disasters and Climate Change in Vietnam, Elsevier, 257–274, https://doi.org/10.1016/B978-0-12-800007-6.00012-5, 2014.

Tantri, E.: (Politic) Dutch Flood Control in Surabaya 1906-1942, pw, 18, https://doi.org/https://doi.org/10.52829/pw.37, 2018.

Trenberth, K. E., Dai, A., Rasmussen, R. M., and Parsons, D. B.: The Changing Character of Precipitation, Bulletin of the American Meteorological Society, 84, 1205–1218, https://doi.org/10.1175/BAMS-84-9-1205, 2003.

Triana, Y. T. and Hidayah, Z.: KAJIAN POTENSI DAERAH RAWAN BANJIR ROB DAN ADAPTASI MASYARAKAT DI WILAYAH PESISIR UTARA SURABAYA, juvenil, 1, 141–150, https://doi.org/10.21107/juvenil.v1i1.6961, 2020.

Vousdoukas, M. I., Mentaschi, L., Voukouvalas, E., Verlaan, M., Jevrejeva, S., Jackson, L. P., and Feyen, L.: Global probabilistic projections of extreme sea levels show intensification of coastal flood hazard, Nat Commun, 9, 2360, https://doi.org/10.1038/s41467-018-04692-w, 2018.

Wahl, T., Jain, S., Bender, J., Meyers, S. D., and Luther, M. E.: Increasing risk of compound flooding from storm surge and rainfall for major US cities, Nature Clim Change, 5, 1093–1097, https://doi.org/10.1038/nclimate2736, 2015.

Ward, P. J., Couasnon, A., Eilander, D., Haigh, I. D., Hendry, A., Muis, S., Veldkamp, T. I. E., Winsemius, H. C., and Wahl, T.: Dependence between high sea-level and high river discharge increases flood hazard in global deltas and estuaries, Environ. Res. Lett., 13, 084012, https://doi.org/10.1088/1748-9326/aad400, 2018.

Wood, M., Haigh, I. D., Le, Q. Q., Nguyen, H. N., Tran, H. B., Darby, S. E., Marsh, R., Skliris, N., and Hirschi, J. J.-M.: Risk of compound flooding substantially increases in the future Mekong River delta, Nat. Hazards Earth Syst. Sci., 24, 3627–3649, https://doi.org/10.5194/nhess-24-3627-2024, 2024.

Yamamoto, K., Habel, S., Son, Y., Anderson, T. R., Obara, C., Barbee, M. M., Fornace, K. L., and Fletcher, C. H.: Compound flood simulations indicate rising public exposure to sewage-contaminated waters in Waikīkī, Hawai'i, Sci Rep, 16, 9740, https://doi.org/10.1038/s41598-026-38225-z, 2026.

Zanaga, D., Van De Kerchove, R., Daems, D., De Keersmaecker, W., Brockmann, C., Kirches, G., Wevers, J., Cartus, O., Santoro, M., Fritz, S., Lesiv, M., Herold, M., Tsendbazar, N.-E., Xu, P., Ramoino, F., and Arino, O.: ESA WorldCover 10 m 2021 v200 (v200), https://doi.org/10.5281/ZENODO.7254221, 2022.

Zscheischler, J., Westra, S., Van Den Hurk, B. J. J. M., Seneviratne, S. I., Ward, P. J., Pitman, A., AghaKouchak, A., Bresch, D. N., Leonard, M., Wahl, T., and Zhang, X.: Future climate risk from compound events, Nature Clim Change, 8, 469–477, https://doi.org/10.1038/s41558-018-0156-3, 2018a.